SORORIN is an evolutionary conserved antagonist of WAPL

Ignacio Prusén Mota[1], Marta Galova[2], Alexander Schleiffer[2], Tan-Trung Nguyen[1], Ines Kovacikova[1], Tomoko Nishiyama[2], Juraj Gregan[1,3,*], Jan-Michael Peters[2,*] and Peter Schlögelhofer[1,*]

1 Department of Chromosome Biology, Max Perutz Labs, University of Vienna, Vienna Biocenter (VBC), Vienna, Austria

2 Research Institute of Molecular Pathology (IMP), Vienna Biocenter (VBC), Vienna, Austria

3 Department of Applied Genetics and Cell Biology, Institute of Microbial Genetics, University of Natural Resources and Life Sciences, Tulln an der Donau, Austria

* Correspondence to:

Peter Schlögelhofer – peter.schloegelhofer@univie.ac.at;

Jan-Michael Peters – Jan-Michael.Peters@imp.ac.at;

Juraj Gregan – juraj.gregan@univie.ac.at

Abstract

Cohesin mediates sister chromatid cohesion to enable chromosome segregation and DNA damage repair. To perform these functions, cohesin needs to be protected from WAPL, which otherwise releases cohesin from DNA. It has been proposed that cohesin is protected from WAPL by SORORIN. However, *in vivo* evidence for this antagonism is missing and SORORIN is only known to exist in vertebrates and insects. It is therefore unknown how important and widespread SORORIN's functions are. Here we report the identification of SORORIN orthologs in *Schizosaccharomyces pombe* (Sor1) and *Arabidopsis thaliana* (AtSORORIN). *sor1Δ* mutants display cohesion defects, which are partially alleviated by *wpl1Δ*. *Atsororin* mutant plants display dwarfism, tissue specific cohesion defects and chromosome mis-segregation. Furthermore, *Atsororin* mutant plants are sterile and separate sister chromatids prematurely at anaphase I. The somatic, but not the meiotic deficiencies can be alleviated by loss of WAPL. These results provide *in vivo* evidence for SORORIN antagonizing WAPL, reveal that SORORIN is present in organisms beyond the animal kingdom and indicate that it has acquired tissue specific functions in plants.

Introduction

Eukaryotic cells perform a complex series of events in order to equally distribute the replicated genome among their daughter cells. DNA replication is not immediately followed by karyokinesis and the newly formed sister chromatids are physically linked for long periods of time until their disjunction during mitosis or meiosis [1,2]. Sister chromatid cohesion (SCC) is mediated by the cohesin complex, which is thought to topologically entrap DNA helices from both newly replicated sisters [3,4]. While SCC promotes chromosome biorientation and DNA damage repair, cohesin can also extrude loops of DNA and facilitate distant intra-chromatid interactions, supporting further roles in chromatin organization and gene expression [5].

Cohesin's core subunits have been identified and characterized in all branches of the eukaryotic kingdom including yeast and plants [6,7]. As a member of the Structural Maintenance of Chromosome (SMC) protein family, cohesin is formed by a heterodimer of SMC1 and SMC3. These proteins fold back on themselves at the hinge domain, where they interact with each other, to form long antiparallel coiled-coil structures. At the other end, their ATPase head domains are bridged together by an α-kleisin subunit, RAD21 (also known as Scc1 or Mcd1) or its meiotic counterparts REC8 and RAD21L [8–10]. These heterotrimeric ring-like structures crucially depend on the recruitment of SCC3 (SA or STAG proteins) to fulfil their chromatin-related functions. SCC3 contributes to cohesin loading, maintenance on chromosomes and its subsequent release from DNA [11–16]. Together, these four proteins form the cohesin core complex.

In addition to SCC3, two further HAWK proteins (HEAT repeat proteins Associated With Kleisin), SCC2 (also known as NIPBL or Mis4) and PDS5 [17], bind to kleisin in a mutually exclusive manner to regulate cohesin behaviour [18,19]. SCC2 is needed to stimulate cohesin's ATPase activity [16,18,20,21] and has been proposed to load cohesin onto DNA [11,22]. *In vitro* experiments have shown that NIPBL is further required for cohesin-mediated loop extrusion [20,21]. PDS5 and WAPL can disrupt the interaction between the SMC3 and kleisin subunits, thereby releasing cohesin from chromatin [23–26]. While cohesin shows a highly dynamic behaviour through cycles of association and release from chromatin, especially during G1, a fraction of cohesin becomes stably bound to DNA after replication and mediates SCC [27,28]. Establishment of cohesion during DNA replication requires acetylation of two lysine residues on SMC3 by the

conserved acetyltransferase Eco1/CTF7 [29–33]. In yeast, Pds5 is required for the acetylation process and for stabilizing cohesin on chromatin [25]. Inactivation of cohesin loading during G1 induces complete cohesin dissociation from DNA in a Wpl1-dependent manner, whereas if inactivation takes place during G2, some cohesin remains chromatin-bound [28]. In *A. thaliana*, mutation of four of the five *PDS5* genes leads to mild defects in meiosis and to severe deficiencies in development, fertility and somatic homologous recombination (HR) [34]. Inactivation of both copies of *WAPL* in *A. thaliana* only mildly affects overall plant development and fertility [35], but rescues the dramatic somatic deficiencies associated with loss of CTF7 [36,37].

In vertebrates and *Drosophila*, an additional protein factor, Sororin, is recruited to the cohesin complex in a replication and SMC3-acetylation dependent manner [38–43]. Sororin promotes SCC until the onset of anaphase by displacing WAPL from PDS5 and counteracting its releasing effects [40]. Both WAPL and Sororin bind to PDS5 through conserved FGF and YSR motifs [40,44].

In somatic cells, Sororin accumulates on chromatin between S and G2 phases and becomes dispersed in the cytoplasm after nuclear envelope breakdown except at centromeric regions where it persists until metaphase [40,42], consistent with its function in promoting SCC [43,45]. This suggests that Sororin, as the cohesin complex, is removed from chromosomes in a stepwise manner [46]. First, the so-called prophase pathway removes chromosomal arm cohesin in a non-proteolytic manner during the first stages of mitosis and meiosis. This process largely depends on WAPL and phosphorylation of STAG2 [13,23,47,48]. Sororin phosphorylation has been proposed to participate in both processes: Cdk1-phosphorylated Sororin may act as a docking protein and recruit Polo-like kinase 1 (Plk1) to mediate STAG2 phosphorylation [49]. Besides, Aurora B and Cdk1 phosphorylate Sororin on several sites and destabilise its association with PDS5, thereby promoting WAPL-mediated removal of cohesion [50,51]. At centromeres, the Shugoshin-PP2A complex protects cohesin from the prophase pathway by keeping Sororin and cohesin subunits in a dephosphorylated state [51–53]. During the metaphase-to-anaphase transition, the anaphase-promoting complex/cyclosome (APC/C^{Cdc20}) targets phosphorylated Securin for degradation to promote the separase-mediated cleavage of the phosphorylated kleisin subunit [42,54–56].

Current data suggest that the main function of Sororin is to counteract the activity of WAPL. While WAPL appears conserved across kingdoms, including yeasts and land

plants, no conserved WAPL antagonist has been described so far. SMC3 acetylation has been proposed to be sufficient to counteract the function of WAPL in organisms thought to lack Sororin, like yeast and plants [37,57]. In *Drosophila melanogaster*, the Sororin-related protein Dalmatian has been characterized [40]. Dalmatian combines protein functions of Sororin and Shugoshin to promote and protect cohesion [41]. Recently, a meiosis I-specific WAPL antagonist (SWI1), that shares no sequence homology to Sororin, has been characterized in *A. thaliana* [58].

To identify possible homologs of *Sororin* we performed a thorough bioinformatics analysis. Our searches revealed putative Sororin relatives in various lower and higher eukaryotes. Here we show that *S. pombe* Sor1 is required for efficient sister chromatid cohesion and that *wpl1* deletion partially suppresses defects caused by the *sor1Δ* mutation. We also demonstrate that Sor1 physically interacts with the cohesin subunit Psm3 (SMC3) and Pds5. We furthermore show, that the *A. thaliana Sororin* homologue (*AtSORORIN*) is essential for vegetative development and microsporogenesis. Lack of AtSORORIN leads to tissue specific reduction or loss of SCC and chromosomal mis-segregation. Consistent with AtSORORIN's proposed function, these somatic phenotypes can be alleviated by loss of WAPL. *Atsororin* mutant plants are sterile, affected in male meiosis with chromatids displaying premature loss of cohesion and splitting of sister-centromeres at anaphase I. Interestingly, the meiotic defects cannot be alleviated by loss of WAPL. Taken together, we provide the first organismal *in vivo* evidence for Sororin antagonizing WAPL function and demonstrate that Sororin is an evolutionary conserved cohesin regulator that has acquired additional functions in plants.

Results

S. pombe Sor1 and *A. thaliana* AtSORORIN share sequence similarities with metazoan Sororin proteins

To identify possible orthologs of *Sororin*, we performed a comprehensive bioinformatics analysis using sensitive remote homology searches. Our searches revealed putative Sororin proteins in both lower and higher eukaryotes including various yeast and plant species. They all show only weak overall sequence conservation with their vertebrate counterparts but they share various characteristic features. The *S. pombe* (SPAC9E9.05) and the *A. thaliana* (At3g56250) gene candidates which both encode short proteins were analyzed in detail. Vertebrate Sororin and Wapl proteins interact with Pds5 through their YSR and FGF motifs [40,44]. Whereas SPAC9E9.05 has a putative FGF motif, such sequence is not present in the plant candidate. A KEN box targets vertebrate Sororin and *Drosophila* Dalmatian for APC/C^{Cdh1}-dependent degradation, but has not been found in either the plant (At3g56250) or the yeast (SPAC9E9.05) candidates. Similar to metazoan Sororin, the proteins encoded by SPAC9E9.05 and At3g56250 have a conserved motif, referred to as the Sororin domain, preceded by a K/R-rich domain at their C-termini (Figure 1a). The Sororin domain has been implicated in interactions with STAG2 and contains two conserved phenylalanine residues important for the maintenance of sister chromatid cohesion (Figure 1b) [59,60].

The *S. pombe* Sororin candidate, SPAC9E9.05, has so far been annotated as a poorly characterized *Schizosaccharomyces* specific protein [61]. Interestingly, a *SPAC9E9.05* deletion mutant was identified in a screen for mutants that showed negative synthetic growth interaction with the cohesion-defective mutants *eso1-G799D* (Eso1 is the *S. pombe* ortholog of Esco1/2 and CTF7 [62]) and *mis4-242* (Mis4 is the *S. pombe* ortholog of NIPBL [63]), suggesting that *SPAC9E9.05* may be involved in regulation of sister chromatid cohesion [64]. Given the similarity of *S. pombe* SPAC9E9.05 and *Arabidopsis* At3G56250 with metazoan Sororin and the data presented below, we decided to name their encoding genes *sor1* (*Sor*orin-like *1*) and *AtSORORIN*, respectively.

S. pombe Sor1 is a nuclear protein involved in sister chromatid cohesion

If *S. pombe* Sor1 was functionally related to mammalian Sororin, then it should be present in the nucleus. Nuclear localization of Sor1 was previously observed when expressed under the control of a strong *nmt1* promoter [65]. To analyze Sor1 localization,

we expressed Sor1-GFP from its native promoter. In an asynchronously growing culture, Sor1-GFP localized to the nucleus in most cells (Supplementary Figure 1a). Immunostaining experiments confirmed the nuclear localization of Sor1-Flag during all tested cell cycle stages (Supplementary Figure 1b).

To assess the role of Sor1 in regulation of cohesion, we analyzed sister chromatid cohesion at the centromeric region (*cen2*-GFP) of chromosome 2. In metaphase, *sor1Δ* mutant cells showed a small, but significant, increase of split sister centromeres (Figure 2a), indicative of a cohesion defect between sister centromeres. However, the role of Sor1 in sister chromatid cohesion is not essential because we observed no defects in chromosome segregation in *sor1Δ* cells (Figure 2b). In mammalian cells, Sororin is dispensable for sister chromatid cohesion in the absence of WAPL [40]. We therefore analyzed sister chromatid cohesion in cells lacking Wpl1, the fission yeast ortholog of WAPL [62]. Interestingly, the increase in split sister centromeres in *sor1Δ* mutant cells was prevented in *sor1Δ wpl1Δ* double mutants (compared to wild type), suggesting that similarly to mammalian cells *wpl1* deletion reduces the sister chromatid cohesion defect caused by the *sor1Δ* mutation (Figure 2a).

Deletion of *sor1* showed negative synthetic growth interaction with both *eso1-G799D* and *mis4-242* mutations but the cause of these defects is unknown [64]. We asked whether defective segregation of chromosomes contributes to this growth defect. Indeed, we observed a higher frequency of lagging chromosomes associated with a higher rate of chromosome mis-segregation in *eso1-G799D sor1Δ* and *mis4-242 sor1Δ* double mutants as compared to single mutants (Figure 2b). This observation is consistent with the role of Sor1 in sister chromatid cohesion regulation.

In telophase and G1, mammalian Sororin is targeted by APC/C for degradation [42]. We therefore tested whether the fission yeast Sor1 is an APC/C substrate, despite the lack of a defined KEN box. We added *in vitro* translated Sor1-HA to interphase *Xenopus* egg extracts in the presence of cycloheximide followed by addition of Cdh1 to activate APC/C^{Cdh1}. We also added *in vitro* translated Sor1-HA to meiotic metaphase-arrested CSF extracts in the presence of cycloheximide followed by addition of $CaCl_2$ to activate APC/C^{Cdc20}. As expected, activation of APC/C^{Cdc20} led to a rapid degradation of the APC/C^{Cdc20} substrate Cyclin B2 and also endogenous *Xenopus* Sororin was degraded within few minutes after activation of APC/C^{Cdh1}. However, we did not observe

187 degradation of *S. pombe* Sor1 by either APC/C^{Cdh1} or APC/C^{Cdc20} (Supplementary
188 Figure 1c).

189 **Conserved residues in the Sororin domain are important for Sor1 function and**
190 **association with cohesin**

191 Mammalian Sororin physically interacts with cohesin and Pds5 and these interactions
192 are essential for Sororin's function [40,59,60]. If the fission yeast Sor1 was an ortholog of
193 metazoan Sororin, Sor1 should interact with cohesin and/or Pds5. We indeed observed
194 that Pds5-Myc co-immunoprecipitated with Sor1-Pk and Sor1-Pk co-
195 immunoprecipitated with Psm3-GFP (Figure 2c, d).

196 The Sororin domain is required for sister chromatid cohesion and association of Sororin
197 with cohesin in mammalian cells [59,60]. To test whether the Sororin domain of *S. pombe*
198 Sor1 is important for its association with cohesin in fission yeast, we analyzed the
199 ability of Psm3-GFP to immunoprecipitate mutant protein Sor1-D303A-Pk, in which a
200 conserved aspartic acid residue D303 in the Sororin domain has been replaced by
201 alanine. Sor1-D303A-Pk co-immunoprecipitated less efficiently with the Psm3-GFP
202 protein, compared to wild type Sor1-Pk, suggesting that the conserved residue D303 in
203 the Sororin domain of Sor1 is important for the association of Sor1 with cohesin (Figure
204 2d).

205 We then asked whether the interaction between *S. pombe* Sor1 and cohesin is
206 functionally relevant. As expected, expression of a wild type Sor1 rescued the growth
207 defect of the *eso1-G799D sor1Δ* double mutant to the level of the *eso1-G799D* single
208 mutant. However, expression of the Sor1-D303A mutant, which weakens the interaction
209 between Sor1 and cohesin, did not restore the growth defect of *eso1-G799D sor1Δ*
210 double mutants (Figure 2e). Mutating three other conserved residues in the Sororin
211 domain of Sor1 (F299A, V302A and Y305A) resulted in a similar phenotype (Figure
212 2e). The observed mutant phenotype was not due to lack of Sor1 expression as all four
213 Sor1 mutant proteins (Sor1-D303A-TAP, Sor1-F299A-TAP, Sor1-V302A-TAP and
214 Sor1-Y305A-TAP) were expressed, although at reduced levels (Supplementary Figure
215 1d).

216 Taken together, we show that fission yeast Sor1 shares similarity with metazoan Sororin
217 proteins. Sor1 is associated with the cohesin complex and *sor1Δ* mutant cells show
218 defects consistent with the role of Sor1 in regulation of sister chromatid cohesion.

Conserved residues at the C-terminus of Sor1 are important for the Sor1 function and its association with cohesin. Unlike metazoan Sororin proteins, Sor1 is not essential for sister chromatid cohesion, suggesting that fission yeast possesses mechanisms that are able to compensate for the absence of Sor1. Our results are consistent with the notion that Sor1 is an ortholog of Sororin in the fission yeast *S. pombe*.

A. thaliana SORORIN is essential for vegetative development and microsporogenesis

Our findings obtained in *S. pombe* motivated us to analyze a Sororin candidate in a non-vertebrate higher eukaryote. The *A. thaliana SORORIN* gene candidate (At3g56250) consists of four exons and codes for a relatively small protein (222 amino acids). Using CRISPR-Cas9 technology we generated a 5 bp deletion in its first exon, creating a premature stop codon (Figure 3a). Heterozygous *Atsororin* +/– plants appear like wild type with only minimally reduced seed numbers, but homozygous mutants display a prominent dwarf phenotype, have few and short siliques and epinastic rosette leaves with short petioles that grow around an undersized stem (Figure 3b). This dramatic phenotype can be complemented with a transgene containing the wild-type gene, including all up- and down-stream regulatory sequences and introns (Supplementary Figure 2a, b), corroborating that the mutation in the *AtSORORIN* gene indeed caused the observed aberrations. Plant roots and shoots develop from meristems, which are formed by actively dividing cells that self-renew and differentiate into new tissue. Root development is severely affected by the lack of AtSORORIN. *Atsororin* mutant plant roots grow significantly shorter than those of wild type, and they completely lose the characteristic layered cellular organization (Figure 3c, d). Moreover, mutant plants are sterile since their short siliques do not develop viable seeds (Figure 3e).

Heterozygous, self-pollinated *Atsororin* +/– plants have less than 4% homozygous *Atsororin* –/– offspring, representing a significant deviation from the expected Mendelian segregation ratio (Figure 3f). Reciprocal crosses between *Atsororin* +/– heterozygous mutant plants and wild type plants revealed that the distortion of segregation ratios is exclusively caused by the male generative cells (Figure 3g). In fact, the morphology of *Atsororin* mutant anthers is abnormal, their size decreased and the amount of shed pollen strongly reduced. A test for pollen viability (Alexander staining) showed that unlike wild-type plants, *Atsororin* mutants produce only very few pollen grains of which only very few are viable (Figure 3h).

Loss of WAPL rescues *Atsororin*-associated defects

In mammalian cells, Sororin is needed to counteract the cohesin-releasing activity of Wapl, and therefore deficiencies related to loss of Sororin can be suppressed by loss of Wapl [40]. Arabidopsis *wapl1-1 wapl2* double mutants exhibit normal vegetative growth and only a mild reduction in fertility (Figure 3b) [35].The *Atsororin*-associated somatic defects can be suppressed by the *wapl1-1 wapl2* double mutant, underlining that Arabidopsis *SORORIN* is a *bona-fide* relative of its vertebrate counterpart. In the *Atsororin wapl1-1 wapl2* triple mutant normal growth of the aerial plant parts and of the roots is restored (Figure 3b-d).

WAPL inactivation only leads to a limited rescue of the fertility defect observed in *Atsororin* mutants. *Atsororin wapl1-1 wapl2* anthers are nearly as small as those of *Atsororin* single mutants and only very few viable pollen grains are formed (Figure 3h). Correspondingly, the triple mutant produces only very few seeds, but still significantly more than the *Atsororin* single mutant (wild type 55 ± 4 seeds/silique (n=74), *wapl1-1 wapl2* 36 ± 9 seeds/silique (n=144; $p<0.0001$), *Atsororin* 0.096 ± 0.35 seeds/silique (n=52; $p<0.0001$); *Atsororin wapl1-1 wapl2* 5 ± 4 seeds/silique (n=166; $p<0.0001$) (Figure 3e).

AtSORORIN is essential in a sub-set of tissues

The data, especially the epistatic relation to *WAPL*, suggested that the gene product of *AtSORORIN* acts in a similar manner as its vertebrate counterpart. We anticipated that the most obvious molecular phenotype of *Atsororin* mutants should be pre-mature loss of sister-chromatid cohesion. To analyze chromosome numbers and sister chromatid cohesion we prepared mitotic cell nuclei samples and specifically stained centromeres (via fluorescent *in situ* hybridization, FISH).

Indeed, interphase nuclei from roots of *Atsororin* mutant plants contain on average 16.82 ± 3.68 centromere signals (n=34). This is significantly more compared to wild type (10.02 ± 0.1458 centromere signals; n=93; $p<0.0001$), *wapl1-1 wapl2* double mutants (10.32 ± 1.66 centromere signals; n=73; $p<0.0001$) and *Atsororin wapl1-1 wapl2* triple mutants (10.49 ± 1.83 centromere signals; n=59; $p<0.0001$) (Figure 4a, b). We attribute the severe mis-organisation of cells in the *Atsororin* mutant roots (Figure 3c) (Supplementary movies 1 – 4) and the arbitrary chromosome numbers in interphase nuclei to massive chromosome mis-segregation due to pre-mature loss of cohesin. Since

the homozygous *Atsororin* mutant plants are under-represented and the mutant root material is scarce and experimentally difficult to process we could only obtain a few cells at metaphase. While in wild-type 10 doublet signals can be seen, in *Atsororin* plants individual chromatids are arranged at the metaphase plate. The anticipated pre-mature loss of SCC leads to random segregation of chromatids during anaphase in *Atsororin* mutants. Importantly, *Atsororin wapl1-1 wapl2* triple mutants are much less affected than the *Atsororin* single mutant (Figure 3c; Figure 4a, b).

Somatic interphase cell nuclei isolated from leaves of *Atsororin* mutant plants, had a close to regular number of chromosomes (10,3 ± 0,5746 centromere signals; n=53), which is still significantly different when compared to wild-type plants (10 centromere signals; n=84; $p<0.0001$), *wapl1-1 wapl2* double mutants (10 centromere signals; n=68; $p<0.0001$) or *Atsororin wapl1-1 wapl2* triple mutants (10 centromere signals; n=82; $p<0.0001$) (Supplementary Figure 2c, d).

We also prepared somatic cells from inflorescences, containing a large number of actively dividing cells that can be readily processed and analyzed (Figure 4c). As for the leaf cells, we established first the number centromeric signals of interphase nuclei. We found, similar to the numbers obtained from leaf cells and in contrast to the ones obtained from root cells, that most cells contain the correct number of chromosomes in *Atsororin* mutants (10.26 ± 1.25 centromere signals; n=266) but still significantly different when compared to wild type (10 centromere signals; n=224; $p<0.0001$), *wapl1-1 wapl2* double mutants (10.01 centromere ± 0.09 centromere signals; n=238; $p<0.0001$) or *Atsororin wapl1-1 wapl2* triple mutants (10.09 centromere signals; n=236; $p<0.0001$) (Figure 4d).

Since a large number of actively dividing cells in anaphase could be observed in the inflorescence tissue we were also in the position to monitor chromosome segregation. In accordance with the mild aberrations of chromosome numbers in interface nuclei, we observed mostly regular chromosome disjunction in *Atsororin* nuclei from inflorescences (97% symmetric disjunction, n=133) with 10 separating chromosomes at either side of the division plane. Those *Atsororin* plants (13/133) that carried 11 chromosomes in all cells, most likely obtained via a gamete with a supernumerary chromosome, showed regular disjunction. In this sense, the occurrence of symmetric divisions was not significantly different from wild-type plants (n=112, p=0.2525) and *wapl1-2 wapl2* (n=119, p=0.9999) and *Atsororin wapl1-2 wapl2* (n=118, p=0.6246)

mutants.

We also measured the inter-sister centromere distance during prophase and prometaphase (Figure 4c, e, f) in somatic cells from inflorescences. Post S-phase 10 doublet signals can be seen in all genotypes tested. While the mutation in *AtSORORIN* does not lead to complete loss of cohesion between sister chromatids, the distance between the 10 centromeric doublet signals is significantly increased compared to wild type (Prophase: 457.6 nm in *Atsororin*, n=39; 378.9 nm in wild type, n=45; $p<0.0001$. Prometaphase: 699 nm in *Atsororin*, n=55; 562.9 nm in wild type, n=42; $p<0.0001$). The sister-centromere distance is, as anticipated, significantly shortened in *wapl1-2 wapl2* mutants compared to wild type (Prophase: 294.2 nm in *wapl1-2 wapl2*, n=37; $p<0.0001$. Prometaphase: 481.4 nm in *wapl1-2 wapl2*, n=43; $p<0.01$). During prophase, the *Atsororin wapl1-2 wapl2* triple mutants have a centromeric distance that is not different from wild type (349.2 nm, n=50; $p=0.2695$), significantly shorter than the *Atsororin* single mutant (457.6 nm, $p<0.0001$) and increased when compared to *wapl1-2 wapl2* mutants (294.2 nm, $p<0.0001$). At prometaphase the centromeric distance of *Atsororin wapl1-2 wapl2* is as tight as in the *wapl1-2 wapl2* mutant (446.1 nm in *Atsororin wapl1-2 wapl2*, n=49; $p=0.4004$). It is interesting to note that in *wapl1-2 wapl2* double mutants, cohesion of sister chromatid arms is maintained in prometaphase since no individual arms can be distinguished. This also holds true in the *Atsororin wapl1-2 wapl2* triple mutant background.

Taken together, we conclude that both AtSORORIN and WAPL impact sister-chromatid cohesion, and that AtSORORIN is not the exclusive antagonist of WAPL activity in all somatic plant tissues.

AtSORORIN is needed for centromeric sister chromatid cohesion during male meiosis

Our analysis indicated that somatic divisions in root cells and microsporogenesis are most severely affected by loss of *AtSORORIN*. To analyze if the underlying cause for the latter can be related to a perturbation of male meiosis we prepared chromosome spreads from meiocytes. Comparing wild-type and *Atsororin* meiocytes it is apparent that AtSORORIN is not an essential factor for sister chromatid cohesion in prophase I. Meiocytes from *Atsororin* plants show normal chromosome condensation and pairing during pachytene and also chiasmata at diakinesis. Bivalents were properly orientated at

the metaphase I plate. Yet, in anaphase I sister chromatids split pre-maturely and were subsequently segregated at random in meiosis II (Figure 5). While in anaphase I / telophase I we observed 5 DAPI-stained bodies at each pole of the dyad in wild type, in *Atsoronin* mutants around 10 DAPI stained bodies can be seen. In metaphase II these 10 DAPI stained bodies could not be aligned properly, were distributed at random during anaphase II and subsequently led to unbalanced tetrads. Supernumerary DAPI stained bodies, which we interpret as individual chromatids, were detected in 71% of *Atsororin* meiocytes during prophase II-metaphase II stages (n=38), while this was never observed in wild type (n=67; $p<0.0001$).

The *wapl1-2 wapl2* double mutants showed strengthened cohesion, characterized by the distinct shape of bivalents at metaphase I, as previously described [35], and regular distribution of chromosomes at meiosis I (n=32) and II. Importantly, in male meiocytes of *Atsororin wapl1-2 wapl2* triple mutants, premature loss of sister chromatids persists. Supernumerary chromatids were observed in 80% of all anaphase I / telophase I meiocytes in the triple mutant (n=40; $p<0.0001$ compared to wild-type or *wapl1-2 wapl2*). This means, that the premature loss of centromeric sister chromatid cohesion at anaphase I / telophase I in *Atsororin* mutants cannot be rescued by loss of WAPL.

To determine the precise timing of loss of sister chromatid cohesion during meiosis of *Atsororin* mutant plants we performed centromeric FISH analysis on meiotic spreads (Figure 6a). As mentioned above, homologous chromosome pairing appeared normal in *Atsororin* mutants, underlined by the presence of 5 dominant CEN signals observed at pachytene stage. During late metaphase I/early anaphase I, five pairs of CEN signals were observed in wild type, with two distinct signals per bivalent (each signal representing two fused sister centromeres) that were orientated to opposite poles. In *Atsororin* mutants, homologous chromosomes showed proper bipolar orientation at metaphase I but the centromeric signals pointing to either pole were often split. All of the observed *Atsororin* metaphases had more than 10 CEN signals (n=24), indicating that sister chromatid centromeres were not fused as in wild type (Figure 6a, b). We quantified the number of centromeric signals observed at metaphase I (including cells from metaphase I to prophase II stages) and metaphase II stages in wild-type plants and *Atsororin*, *wapl1-2 wapl2* double and *Atsororin wapl1-2 wapl2* triple mutants (Figure 6c, d). While meiocytes from wild-type and *wapl1-2 wapl2* mutant plants did mostly not suffer from premature splitting of sister-centromeres at metaphase I (93.4% and

91.3% of cells with 10 centromere signals respectively, n=76 in wild type, n=23 in *wapl1-2 wapl2*; p=0.6622) and had perfectly paired sister-centromeres at metaphase II (n=17 in wild type, n=10 in *wapl1-2 wapl2*), Atsororin and *Atsororin wapl1-2 wapl2* mutants displayed split sister-centromere signals at metaphase I (n=24, p<0.0001 in *Atsororin*; n=31, p<0.0001 in the triple mutant), and non-paired sister-centromeres at metaphase II (n=13, p<0.0001 in *Atsororin*; n=17, p<0.0001 in *Atsororin wapl1-2 wapl2* mutants).

As mentioned above, after loss of sister chromatid cohesion, progression through meiosis II is compromised and in *Atsororin* and *Atsororin wapl1-2 wapl2* mutants individual chromatids segregated at random. We quantified tetrads with balanced chromosome numbers (Figure 6e). While in wild-type plants, all meiocytes generated balanced tetrades (n=33), none of the *Atsororin* mutants produced balanced tetrades (n=25; p<0.0001), *wapl1-2 wapl2* mutants produced 75% of balanced tetrades (n=28; p<0.01) and *Atsororin wapl1-2 wapl2* none (n=18; p<0.0001). These observations lend further support to the notion that the meiotic deficiencies in AtSORORIN cannot be rescued by loss of WAPL.

It Is interesting to note that while univalent chromosomes were not observed in WT or *wapl1-1 wapl2* mutants, a significant fraction (13%) of *Atsororin* meiocytes showed presence of an extra univalent chromosome (scored at diakinesis-metaphase I stages; n=53; p<0.01). Presence of extra chromosomes could be the consequence of a previous non-disjunction event in the meiocyte precursor cells, or the result of fertilization between unbalanced generative cells (see also above). Interestingly, we did not observe univalents in the *Atsororin wapl1-1 wapl2* triple mutants (n=32).

AtSORORIN does not affect meiotic cohesin abundance and axis formation in meiotic prophase

We were curious to understand AtSORORIN's impact on cohesion abundance in a severely affected tissue. We therefore performed chromosome spreads of male meiocytes and subsequent immune-staining using antibodies directed against the cohesin subunit SCC3 and the meiosis specific kleisin subunit REC8 (Figure 7; Supplementary Figure 3). We scored cells at the zygotene/pachytene transition as cohesins can still be observed well at this stage. To correctly stage progression of meiosis, we also detected the meiotic axis component ASY1 and the transverse filament

protein of the synaptonemal complex (SC), ZYP1. Our analysis shows that during meiotic prophase, axis formation, as judged from the ASY1 signal, and SC formation, as judged from the ZYP1 signal, is indistinguishable from wild type in *Atsororin*, *wapl1-2 wapl2* and *Atsororin wapl1-2 wapl2* mutants. Furthermore, cohesion abundance and deposition, as judged from the SCC3 and REC8 signals, along the chromosome arms appears unaffected in *Atsororin*, *wapl1-2 wapl2* and *Atsororin wapl1-2 wapl2* mutants (Figure 7; Supplementary Figure 3).

Discussion

Cohesin complexes are evolutionarily ancient inventions of nature, involved in proper chromosome disjunction in mitosis and meiosis, but also essential for chromosome organization [66]. In animal cells, Wapl has been recognized as a cohesin removal factor which itself is kept in check by the antagonizing protein Sororin [23,40,45]. While cohesion complex proteins, Wapl and Eco1-dependent acetylation of cohesin are conserved from yeast and plants to humans, Sororin was thought to be present only in metazoans [5,41]. A Sororin-like protein has been characterized in the fly, with a peculiar dual function; it serves as a Wapl antagonist and also as a centromeric cohesion protector [40,41]. In *Arabidopsis*, the protein SWI1 antagonizes the function of WAPL, but exclusively only during meiotic prophase I, and it shares no sequence homology with the vertebrate or fly relatives [58,67]. These results suggested that WAPL antagonists should also be present in the genomes of other eukaryotes, but possibly strongly diverged in sequence or occurring as functional domain in the context of larger proteins.

Applying sensitive remote homology searches, we identified putative Sororin relatives in various organisms, including *S. pombe* and *A. thaliana*, which are separated by approximately 1.5 billion years of independent development.

We show that Sor1, the *S. pombe* Sororin-relative, physically interacts with cohesin (via SMC3/Psm3) and Pds5. However, we observed only a mild sister chromatid cohesion defect in *sor1Δ* cells, suggesting that there are other mechanisms that compensate for the absence of Sor1. Importantly, *wpl1* deletion partially suppressed the sister chromatid cohesion defect caused by the *sor1Δ* mutation, suggesting that, similarly as metazoan Sororin, Sor1 antagonizes the function of Wapl. Our results are consistent with the notion that Sor1 is an ortholog of Sororin in the fission yeast *S. pombe*.

Conversely, the *Arabidopsis* Sororin relative is an important factor for plant viability and vigor. *Atsororin* mutant plants are underrepresented in segregating populations due to compromised male, but not female, transmission of the mutant allele. The few plants that develop with a homozygous *Atsororin* mutation are dwarfed, have a short and distorted root and are sterile. Interestingly, among the somatic tissues analyzed, only roots show a strong chromosome mis-segregation phenotype, while other tissues are less affected. Somatic cells from inflorescences show hardly any mis-segregation but a widening of centromeric distances in prophase/pro-metaphase, compatible with

AtSORORIN's role in limiting WAPL's activity. *Atsororin* plants are sterile and the main underlying cause appears to be premature loss of sister centromere cohesion at anaphase I during male meiosis. This is different from the defect observed in *swi1* mutants, with premature loss of sister chromatid cohesion in early meiotic prophase I [58]. Importantly, the somatic defects of *Atsororin* mutants and the meiotic defect of *swi1* mutants could be rescued in the absence of WAPL (*wapl1 wapl2* double mutants), while the meiotic defects of *Atsororin* could not be alleviated.

It is interesting to note, that a very similar phenotype compared to *Atsororin* has been observed in the acetyltransferase mutant *CTF7* [36], a relative of Eco1 and ESCO1/2 [31,68]. Eco1/CTF7 acetylates the cohesin subunit SMC3 during DNA replication, thereby promoting recruitment of SORORIN and antagonizing the function of WAPL [38–40]. In plants, inactivation of WAPL in a *ctf7* mutant background restores somatic growth but fails to fully rescue the *ctf7* fertility defect [37]. These results indicate that first, AtSORORIN and AtCTF7 may act in the same pathway to promote sister chromatid cohesion by antagonizing WAPL, and second, that the dramatic dwarf phenotype observed in the single *Atsororin* and *ctf7* mutants is not a direct effect of the respective mutation, but an indirect, possibly mediated by altered cohesin dynamics.

Sororin has initially been perceived as the only WAPL antagonist in vertebrates [40], but later the histone kinase Haspin has also been described as a WAPL antagonist with respect to cohesive cohesin [69,70]. It is interesting to note that loop extruding cohesin is also protected from WAPL by CTCF [71,72]. Haspin has been implicated in centromeric localization of the chromosome passenger complex (CPC) which plays a crucial role in chromosome bi-orientation by correcting erroneous microtubule attachment [73]. Localization of the CPC relies on histone H3-T3 phosphorylation, which is mediated by the histone kinase Haspin/Hrk1 [74–76]. Hrk1/Haspin localization to centromeres depends on its interaction with Pds5 [70,77,78].

In this sense, the protein PDS5 has emerged as a central regulator for the orchestration of cohesin dynamics. Via its conserved A P D/E A P motif [44,78], it can interact with diverse regulators. In human cells, PDS5 utilises this motif to interact with WAPL, HASPIN and SORORIN. Importantly, the three proteins share a common PDS5-interaction motif (PIM: K/R T/S Y S R K/L) and compete for PDS5 binding [44,69,70]. Furthermore, *S. pombe* Pds5 has been characterized to interact with Wpl1, Hrk1 and Eso1 (with the latter two inhibiting cohesin removal) [78]. Also these three proteins have a

common Pds5-interaction motif [78] and compete for the same binding domain on Pds5. Here we demonstrate that yet another protein, Sor1, can interact with Pds5, potentially also competing for the same binding platform.

Arabidopsis has five *PDS5* genes [34], of which three encode PDS5 variants with a perfectly conserved interaction motif. The two *A. thaliana* WAPL proteins have well conserved PIMs at their N-termini (R T Y G R R) and are very likely direct interaction partners of PDS5 proteins, with experimental proof for the WAPL1-PDS5A pair [58].

Common to all SORORIN proteins is the Sororin domain [60]. Previously it was shown to be important for interaction with cohesin complexes (SA2) and the maintenance of sister chromatid cohesion [59,60]. The Sororin domain is well-conserved in the *A. thaliana* and in *S. pombe* relatives, yet only one phenylalanine is present within the motif of the latter. We established in *S. pombe* that mutating this residue (F299) to alanine is as detrimental as a complete deletion of the *sor1* gene.

Interestingly, while we could not identify a putative PIM in the *A. thaliana* Haspin protein we noticed a well-conserved Sororin domain (Y F R D I D A F E), which is not present in Haspin proteins from other organisms. In this sense, plant Haspin may be localised to cohesin via interacting with the SCC3 subunit and may also play a role as WAPL antagonist in plants.

Importantly, our study provides the first organismal *in vivo* evidence that SORORIN antagonizes WAPL. We conclude (1) that orthologs of SORORIN are wide-spread in eukaryotes including yeast and plant species; (2) that plants encode more than one WAPL antagonist, and (3) that they act in clearly defined tissue and developmental contexts; and (4) that AtSORORIN may have acquired, similar to *Drosophila*'s Dalmatian, additional WAPL-independent functions in sister centromere protection at the meiosis I to meiosis II transition.

Material and methods

Bioinformatic analyses

Sororin orthologs are characterized by a very short domain at the C-terminus, which is shared between mammals and insects. This region consists of a stretch of positively charged amino acids, a polar linker (varies in size between 10 and 20 amino acids) and a conserved motif predicted to form two alpha helices and a beta strand [40]. We could not expand the Sororin protein family to other taxonomic clades such as fungi or plants when we considered only statistically significant hits (e-value 1e-2, data not shown). To identify candidates in other model organisms we used a hidden Markov model (HMM) of the C-terminal region (covering the *Homo sapiens* Sororin protein gi|18087845|ref|NP_542399.1|: 216-252) and searched specifically in the proteomes of *Saccharomyces cerevisiae* and *Schizosaccharomyces pombe* (HMMER suite version 2.3.2) [79]. We received 26 (*S. cerevisiae*) and 28 (*S. pombe*) hits with low significant e-values between 0.78 and 10. The hits were manually filtered according to the following criteria: location of the alignment at the C- terminus, conservation of the hydrophobic pattern (especially the phenylalanine residues), and no overlap with known functional domains. In budding yeast, no hit fulfilled all these criteria. In fission yeast, the best hit was to the protein SPAC9E9.05.1 (e-value 1, score -4.0). The protein is 313 residues long and the HMM alignment spanned from 241 to 310. SPAC9E9.05.1 is specific to the *Schizosaccharomyces* genus - no other orthologs could be detected with a NCBI-blastp search (version 2.2.26) [80] besides in *Schizosaccharomyces cryophilus*, *Schizosaccharomyces octosporus*, and *Schizosaccharomyces japonicus*. The conservation within the SPAC9E9.05 protein family is very poor (overall *S. pombe* and *S. japonicus* are only 23% identical), the C-terminus being the highest conserved region (30% identical). No known functional domains could be detected in the PFAM database. We incorporated the SPAC9E9.05.1 *Schizosaccharomyces* sequences into the HMM model and extended the search to other fungi species. In the proteome of the ascomycete *Pyrenophora tritici-repentis* (strain Pt-1C-BFP), the best hit was to a predicted protein (gi|189210197|ref|XP_001941430.1|, score 13.5, e-value 0.089) belonging to an uncharacterized protein family that is conserved within the *Pezizomycotina clade*.

We confined the HMM-model to a region with highest conservation (*S. pombe* SPAC9E9.05.1: 298-311), using only fungi proteins, and searched specifically in

Saccharomycetes species. In *Lipomyces starkeyi*, the best hit was significant (jgi|Lipst1_1|72111|Locus1483v3rpkm29.51, e-value 0.0041, score 20.9) and located at the c-terminus as well. Similarly, in the *Yarrowia lipolytica* proteome we selected YALI0C19756p (e-value 0.03, score 17.7). However, no candidate could be identified in *Saccharomyces cerevisiae* or in *Candida species*.

To identify plant candidates, we used the same HMM model as for the *S. pombe* screen before and searched within the *Arabidopsis thaliana* proteome. The best hit was to an unknown protein (AT3G56250.1, e-value 0.04, score 14.7), which is a member of a plant specific protein family. Like for the Sororin family and the fungi candidates, the highest conservation lies in the C-terminal region. Except for some plant species, such as *Oryza sativa Japonica*, only one candidate gene was identified per genome.

The proteomes used in this study were retrieved from the NCBI-protein database (http://www.ncbi.nlm.nih.gov/protein) besides for *Saccharomyces cerevisiae* (http://www.yeastgenome.org/), *Schizosaccharomyces pombe* (http://www.pombase.org/), *Lipomyces starkeyi* (http://genome.jgi.doe.gov/Lipst1_1) and *Arabidopsis thaliana* (http://www.arabidopsis.org/).

Mulitple alignments were performed with MAFFT (version 7, L-INS-I method) [81], secondary structure prediction with Jpred (v4) [82]; and analyzed in Jalview [83].

S. pombe methods

The genotypes of *S. pombe* strains used in this study are listed in Table 1. Standard YES media were used to grow *S. pombe* strains strains [84–86]. Tagging and deletion of *S. pombe* genes was performed according to our protocols described in [87] and [88], respectively. The immunofluorescence and microscopy techniques used to analyze chromosome segregation were performed as described in [89]. Point mutations in the *sor1* gene (to yield sor1-F299A, sor1-V302A, sor1-D303A and sor1-Y305A variants proteins) were introduced into the cloned *sor1* gene using the QuikChangeII kit (Agilent Technologies) and inserted into the genome by transformation.

For Western blot analyses, proteins were separated by electrophoresis through 12% polyacrylamide gels containing SDS (0.1%) and transferred to a PVDF membrane (Millipore). The membrane was blocked with 2% (w/v) milk-PBS-T (phosphate buffer saline buffer with 0.1% (v/v) Tween-20) and probed with antibodies. TAP-tagged

proteins were detected using rabbit antiperoxidase antibody linked to peroxidase (PAP, Dako; 1:10000 dilution). Tubulin was detected using mouse-anti-α-tubulin antibody (Sigma-Aldrich T5168; 1:10000 dilution) and rabbit anti-mouse IgG-HRP secondary antibody (Santa Cruz Biotechnology; 1:5000 dilution). GFP-tagged proteins were detected using mouse anti-GFP antibody (Roche 1814460, 1:1000 dilution) and anti-mouse-HRP antibody (Amersham, 1:5000). PK-tagged proteins were detected using mouse-anti-PK (V5) antibody (Serotec; 1:2000 dilution) and goat anti-mouse IgG-HRP secondary antibody (Santa Cruz Biotechnology; 1:5000 dilution) in 0.1% PBS-T. Myc-tagged proteins were detected using rabbit c-Myc antiserum (CM-100, Gramsch, Germany, 1:10000 dilution) and secondary mouse anti-rabbit-IgG antibody conjugated to HRP (sc-2357, Santa Cruz Biotechnology, 1:20000 dilution).

For coimmunoprecipitation, 10 ml of exponentially growing cells were collected, washed and lysed in 300 µL of IPP150 buffer [50 mM Tris-Cl (pH=8.0), 150 mM NaCl, 10% glycerol, 0.1% NP-40, 1 mM PMSF and complete EDTA-free protease inhibitors] using glass beads as described in [90]. The lysates were centrifuged and subjected to affinity purification via binding to anti-V5 agarose beads (Sigma-Aldrich) for 1 hour at 4°C. After washing with IPP150 buffer (3x1.5 ml), the bound proteins were released by the addition of SDS–PAGE sample buffer at 95°C for 3 min. The presence of tagged proteins in the immunoprecipitates was detected by Western blot analysis as described above.

In vitro APC/C assay in *Xenopus* egg extracts was performed as previously described [40].

Plant mutant lines and growth conditions

The *Arabidopsis thaliana* Columbia (Col-0) ecotype was used as wild-type reference. *Atsororin* mutant plants were generated via CRISPR-Cas9 (see below). The *wapl1-1 wapl2* double mutant (SALK_108385, SALK_127445) [35] was crossed with heterozygous *AtSORORIN* +/- mutant to obtain the *Atsororin wapl1-1 wapl2* triple mutant. Plants were grown on soil or in media plates containing Murashige and Skoog agar medium [91] with 2% sucrose. Long day growth conditions were applied with cycles of 16 hours light and 8 hours dark, at 21°C and 60% humidity.

Leaves from rosette-stage plants grown on soil or the first true leaves from seedlings grown on plates, were collected for DNA isolation and genotyping. Mutants were

confirmed by PCR using the primers listed below (Table 2). *Atsororin* mutants were confirmed by Sanger Sequencing of the PCR product.

Floral dip transformation of *A. thaliana*

Arabidopsis was transformed via *Agrobacterium tumefaciens* mediated DNA transfer. In brief, an aliquot of *A. tumefaciens* electroporation-competent cells was thawed on ice and 100 ng of plasmid were added. After 15 minutes incubation on ice, the cells were transferred to electroporation cuvettes (Eppendorf, 4307-000-593). After electroporation (400 Ω, 25 µF, 2.5 kV), 900 µL of SOC media were added to the cuvettes and cells were left to rest for 1 hour at RT. 300 µL of transformed cells were plated on 2xTY plates supplemented with 50 µg/ml gentamycin, 50 µg/ml rifampicin and 100 µg/ml kanamycin (plasmid selection). Plates were left at 30ºC overnight.

A single colony from transformed *Agrobacterium tumefaciens* was inoculated into 500 mL of 2xTY medium supplemented with antibiotics. After 2 days rotating at 30ºC, cells were centrifuged at 4500g for 30 minutes at 4ºC. The pellet was then resuspended in 200 mL infiltration buffer (5% sucrose in dH_2O). Another centrifugation at 4500g for 30 minutes at 4ºC was performed and cells were now resuspended in 200 mL infiltration buffer containing 40 µL Silwet-L77. Prior to dipping the plants into the solution, their already developed siliques and open flowers were removed. Plants were then dipped into the Agrobacterium/infiltration buffer solution for 30 seconds and wrapped into plastic bags afterwards to avoid fast drying of the bacterial solution. Plants were transferred to the growth chamber and two days later the bags were removed.

Atsororin mutant generation

The *Atsororin* mutant was generated by using the CRISPR-CAS9 technology. The gRNA sequence 5'-CCGTCGGAGGAAGAATACAG-3' is specific to exon 1 of the *ATSORORIN* gene (At3g56250) and induces cleavage a few nucleotides downstream of the ATG codon. The gRNA was cloned into pGGE000-EF_pChimera2, and together with the Cas9 promoter in pGGA000-AB_PcUbi, the Cas9 version in pGGB000-BC_PuCas9 and the Cas9 terminator in pGGC000-CD_PeaTer further subcloned into the destination vector pGGZ003 utilizing the GOLDENGATE technique. The final plasmid was used to transform *Col*-0 plants by using the floral dip method [92]. Transgenic plants grown on soil were identified and selected by their resistance to the herbicide Basta (applied by spraying 13.5 mg/l). For subsequent generations we

screened for the absence/presence of the BASTA resistance gene (*PAT*) using the primers 35Sp_Fwd and Basta_Rev. Offspring of the initial transformants with or without the transgene were analysed for the presence of a mutation in the first exon 1 of the *AtSORORIN* gene. To do so, PCR amplicons were generated using the primers Sororin_geno_Fwd and Sororin_geno_Rev and subsequently sequenced with the primer Sororin_sequencing (Table 2). Plants with a mutation signature were grown for one or two more generations to identify individuals that inherited the mutation. We finally obtained a line without transgene and a stable heterozygous mutation in the *AtSORORIN* gene (Figure 1). The *Atsororin* mutant line contains a 5bps deletion within the first exon, 25 nucleotides down-stream of the ATG start codon. It results in a premature TAA stop codon after generating a short peptide of 18 amino acid residues.

Complementation of *Atsororin* mutation

For complementing the *Atsororin* mutation, we first amplified the wild type *AtSORORIN* genomic version of the gene by PCR using Phusion DNA Polymerase. The primers specific for the amplification are listed in Table 2. The amplicon was then cloned into the pCB302 vector [93], which is compatible with *A. tumefaciens* transformation and contains the BASTA resistance gene for future plant selection. Heterozygote *AtSORORIN* +/- plants were transformed with the pCB302 vector containing the *AtSORORIN* gene by the floral dip method to obtain the T1 generation of transformant plants. Two weeks old plants were selected for positive transformants by spraying the herbicide BASTA (150 mg/L BASTA in H_2O). Heterozygote *AtSORORIN* +/- plants (based on sequencing) and BASTA-resistant were selected for three more generations. The offspring of several F3 plants were sown on soil to check their genotype. The analyzed *Atsororin* complementation lines were those that only generated offspring containing the *Atsororin* mutant allele and the complementing transgene (parent plants were homozygous for both, the *Atsororin* mutant allele and the complementing transgene).

Seed counts

Mature but still green siliques originating from the fifth to the thirtieth flower per stem were harvested into fixing solution (1 part of glacial acetic acid and 3 parts of 96% EtOH) for distaining. After one day, the solution was renewed and seeds inside siliques were counted manually under a binocular microscope.

Alexander staining [94]

For pollen viability assays, the anthers and pollens from mature flowers were dissected under the microscope. The individual anthers were placed on a slide and a few drops (~20 µl) of Alexander staining buffer (500 µl of water, 250 µl of 87% glycerin, 100 µl of 96% Ethanol, 50 µl of 1% acid fuchsin, 10 µl of 1% malachite green, 5 µl of 1% orange G, 50 µl of glacial acetic acid) were added. The anthers were covered with a coverslip and the microscopic slide was then incubated at 50ºC overnight. Stained pollen grains were observed with a microscope equipped with a differential contrast interference microscopy optics. Viable pollen grains appear round, filled with red-stained cytoplasm and coated with a thin green layer, while non-viable pollen appear only green, often shriveled and lack red cytoplasm.

Spreading of nuclei, fluorescence *in situ* hybridisation (FISH) and immunolocalization of meiotic proteins

For somatic cell preparations, the tissue of interest was fixed in Carnoy´s fixative (1 part of glacial acetic acid and 3 parts of 96% EtOH). After washings twice with TRIS buffer (10mM TRIS pH 7.5, 10mM EDTA, 100mM NaCl), the plant material was disrupted with a plastic pestle in Lysis buffer (15mM TRIS pH7.5, 0,5mM spermine, 2mM EDTA, 80mM KCl, 20mM NaCl, 0,1% Triton X-100). The solution was then pipetted trough a 40-micron cell strainer and centrifuged at 500g for 3 minutes. The pellet was resuspended in 50 µL of lysis buffer and pipetted to a glass slide to let air-dry. In order to visualize meiotic progression, anther spreads were prepared as described in [95]. Fluorescence *in situ* hybridization (FISH) was performed as described in [96]. In brief, slides with somatic or meiotic nuclei were washed twice with 2xSSC for 5 minutes. After 10 minutes in 4% paraformaldehyde, slides were quickly washed in water and transferred through an ethanol series (70%, 90% and 96% EtOH) and then left to dry. A Locked Nucleic Acid (LNA) probe was used to detect centromere regions (5'-TTGGCTACACCATGAAAGCTT-3'; Qiagen). 20 µL of probe mix (250 nM LNA probe, 10% dextran sulfate, 50% formamide in 2 x Saline Sodium Citrate) were pipetted on the slide. A coverslip was applied, and the slides were placed on a hot plate at 75ºC for 4 minutes. After an overnight incubation at 37ºC, the slides were washed twice in 2xSCC and 15 µL of 2 µg/ml 4',6 diamidino-2-phenylindol (DAPI) diluted in Vectashield (Vector Laboratories) were applied.

Spreads of nuclei for the detection of meiotic chromatin and associated proteins were

performed as previously described [97]. Primary antibodies were used as follows: 1:10000 anti-ASY1 raised in guinea pig [96], 1:500 anti-ZYP1 raised in rat [98], 1:500 anti-SCC3 raised in rabbit [99] and 1:250 anti-REC8 raised in rabbit [100]. The secondary antibodies are all commercially available and were used as follows: anti-guinea pig conjugated to Alexa Fluor 488 (1:400), anti-rabbit conjugated to Alexa Fluor 568 (1:400) and anti-rat conjugated to Alexa Fluor 647 (1:200).

Images were obtained with a Zeiss Axioplan microscope (Zeiss, Oberkochen, Germany) using a Quantix® CCD camera (Photometrics, Tucson, U.S.A.). Picture acquisition was performed with MetaMorph® Micoscopy Automation & Image Analysis software (Molecular Devices, Sunnyvale, U.S.A.). For meiotic prophase nuclei, Z-stacks with 100 nm intervals were acquired. Deconvolution was performed using AutoQuant software (Media Cybernetics Inc, Rockville, U.S.A.) and projections were done using Helicon Focus software (HeliconSoft, Kharkov, Ukraine).

Root tip image processing

Whole roots from 2-weeks old plants grown on plates were collected from different genotypes and immersed in a solution of 10 µg/mL DAPI with 0,1% Triton-X100. After 30 minutes incubation at room temperature, roots were placed on a slide.

Imaging was performed with a Zeiss LSM710 microscope equipped with an AiryScan Unit. To generate the movies, Z-stacks with 250 nm intervals were acquired. Deconvolution was performed with the Huygens Software.

Statistical analyses

All statistical analyses were performed using the GraphPad Prism 7 software. First, D'Agostino-Pearson omnibus normality test was performed to analyze if the data followed a Gaussian distribution. If yes, the two variables were compared using unpaired t-test. When no Gaussian distribution was detected, unpaired Mann-Whitney tests were applied. Contingency tables were generated to compare expected (or wild type) data with mutant values. Fischer's exact test was used when two variables were compared. For three or more variables, Chi-square tests were performed.

References

1. Ishiguro, K. ichiro. The cohesin complex in mammalian meiosis. *Genes to Cells* vol. 24 6–30 (2019).
2. Oldenkamp, R. & Rowland, B. D. A walk through the SMC cycle: From catching DNAs to shaping the genome. *Molecular Cell* vol. 82 1616–1630 (2022).
3. Haering, C. H., Farcas, A. M., Arumugam, P., Metson, J. & Nasmyth, K. The cohesin ring concatenates sister DNA molecules. *Nature* **454**, 297–301 (2008).
4. Peters, J. M., Tedeschi, A. & Schmitz, J. The cohesin complex and its roles in chromosome biology. *Genes Dev.* **22**, 3089–3114 (2008).
5. Davidson, I. F. & Peters, J. M. Genome folding through loop extrusion by SMC complexes. *Nature Reviews Molecular Cell Biology* vol. 22 445–464 (2021).
6. Tomonaga, T. *et al.* Characterization of fission yeast cohesin: Essential anaphase proteolysis of Rad21 phosphorylated in the S phase. *Genes Dev.* **14**, 2757–2770 (2000).
7. Schubert, V. SMC proteins and their multiple functions in higher plants. *Cytogenetic and Genome Research* vol. 124 202–214 (2009).
8. Schleiffer, A. *et al.* Kleisins: A superfamily of bacterial and eukaryotic SMC protein partners. *Mol. Cell* **11**, 571–575 (2003).
9. Gligoris, T. G. *et al.* Closing the cohesin ring: Structure and function of its Smc3-kleisin interface. *Science (80-.).* **346**, 963–967 (2014).
10. Sonoda, E. *et al.* Scc1/Rad21/Mcd1 Is Required for Sister Chromatid Cohesion and Kinetochore Function in Vertebrate Cells. *Dev. Cell* **1**, 759–770 (2001).
11. Hu, B. *et al.* ATP hydrolysis is required for relocating cohesin from sites occupied by its Scc2/4 loading complex. *Curr. Biol.* **21**, 12–24 (2011).
12. Orgil, O. *et al.* A Conserved Domain in the Scc3 Subunit of Cohesin Mediates the Interaction with Both Mcd1 and the Cohesin Loader Complex. **11**, e1005036 (2015).
13. Hauf, S. *et al.* Dissociation of cohesin from chromosome arms and loss of arm cohesion during early mitosis depends on phosphorylation of SA2. *PLoS Biol.* **3**, (2005).
14. Roig, M. B. *et al.* Structure and function of cohesin's Scc3/SA regulatory subunit. *FEBS Lett.* **588**, 3692–3702 (2014).
15. Li, Y. *et al.* Structural basis for scc3-dependent cohesin recruitment to chromatin. *Elife* **7**, (2018).
16. Murayama, Y. & Uhlmann, F. Biochemical reconstitution of topological DNA binding by the cohesin ring. *Nature* **505**, 367–371 (2014).
17. Wells, J. N., Gligoris, T. G., Nasmyth, K. A. & Marsh, J. A. Evolution of condensin and cohesin complexes driven by replacement of Kite by Hawk proteins. *Current Biology* vol. 27 R17–R18 (2017).
18. Petela, N. J. *et al.* Scc2 Is a Potent Activator of Cohesin's ATPase that Promotes Loading by Binding Scc1 without Pds5. *Mol. Cell* **70**, 1134-1148.e7 (2018).
19. Kikuchi, S., Borek, D. M., Otwinowski, Z., Tomchick, D. R. & Yu, H. Crystal structure of the cohesin loader Scc2 and insight into cohesinopathy. *Proc. Natl. Acad. Sci. U. S. A.* **113**, 12444–12449 (2016).
20. Davidson, I. F. *et al.* DNA loop extrusion by human cohesin. *Science (80-.).* **366**, 1338–1345 (2019).

773 21. Kim, Y., Shi, Z., Zhang, H., Finkelstein, I. J. & Yu, H. Human cohesin compacts DNA by loop
774 extrusion. *Science (80-.).* **366**, 1345–1349 (2019).

775 22. Ciosk, R. *et al.* Cohesin's binding to chromosomes depends on a separate complex consisting of
776 Scc2 and Scc4 proteins. *Mol. Cell* **5**, 243–254 (2000).

777 23. Kueng, S. *et al.* Wapl Controls the Dynamic Association of Cohesin with Chromatin. *Cell* **127**,
778 955–967 (2006).

779 24. Beckouët, F. *et al.* Releasing Activity Disengages Cohesin's Smc3/Scc1 Interface in a Process
780 Blocked by Acetylation. *Mol. Cell* **61**, 563–574 (2016).

781 25. Chan, K. L. *et al.* Cohesin's DNA exit gate is distinct from its entrance gate and is regulated by
782 acetylation. *Cell* **150**, 961–974 (2012).

783 26. Huis In't Veld, P. J. *et al.* Characterization of a DNA exit gate in the human cohesin ring. *Science*
784 *(80-.).* **346**, 968–972 (2014).

785 27. Gerlich, D., Koch, B., Dupeux, F., Peters, J. M. & Ellenberg, J. Live-Cell Imaging Reveals a Stable
786 Cohesin-Chromatin Interaction after but Not before DNA Replication. *Curr. Biol.* **16**, 1571–1578
787 (2006).

788 28. Bernard, P. *et al.* Cell-cycle regulation of cohesin stability along fission yeast chromosomes.
789 *EMBO J.* **27**, 111–121 (2008).

790 29. Ben-Shahar, T. R. *et al.* Eco1-dependent cohesin acetylation during establishment of sister
791 chromatid cohesion. *Science (80-.).* **321**, 563–566 (2008).

792 30. Ivanov, D. *et al.* Eco1 is a novel acetyltransferase that can acetylate proteins involved in
793 cohesion. *Curr. Biol.* **12**, 323–328 (2002).

794 31. Tóth, A. *et al.* Yeast cohesin complex requires a conserved protein, Eco1p(Ctf7), to establish
795 cohesion between sister chromatids during DNA replication. *Genes Dev.* **13**, 320–333 (1999).

796 32. Ünal, E. *et al.* A molecular determinant for the establishment of sister chromatid cohesion.
797 *Science (80-.).* **321**, 566–569 (2008).

798 33. Zhang, J. *et al.* Acetylation of Smc3 by Eco1 Is Required for S Phase Sister Chromatid Cohesion in
799 Both Human and Yeast. *Mol. Cell* **31**, 143–151 (2008).

800 34. Pradillo, M. *et al.* Involvement of the cohesin cofactor PDS5 (SPO76) during meiosis and DNA
801 repair in Arabidopsis thaliana. *Front. Plant Sci.* **6**, 1034 (2015).

802 35. De, K., Sterle, L., Krueger, L., Yang, X. & Makaroff, C. A. Arabidopsis thaliana WAPL Is Essential for
803 the Prophase Removal of Cohesin during Meiosis. *PLoS Genet.* **10**, e1004497 (2014).

804 36. Bolaños-Villegas, P. *et al.* Arabidopsis CHROMOSOME TRANSMISSION FIDELITY 7 (AtCTF7/ECO1)
805 is required for DNA repair, mitosis and meiosis. *Plant J.* **75**, 927–940 (2013).

806 37. De, K. *et al.* The opposing actions of arabidopsis CHROMOSOME TRANSMISSION FIDELITY7 and
807 WINGS APART-LIKE1 and 2 differ in mitotic and meiotic cells. *Plant Cell* **28**, 521–536 (2015).

808 38. Lafont, A. L., Song, J. & Rankin, S. Sororin cooperates with the acetyltransferase Eco2 to ensure
809 DNA replication-dependent sister chromatid cohesion. *Proc. Natl. Acad. Sci. U. S. A.* **107**, 20364–
810 20369 (2010).

811 39. Song, J. *et al.* Cohesin acetylation promotes sister chromatid cohesion only in association with
812 the replication machinery. *J. Biol. Chem.* **287**, 34325–34336 (2012).

813 40. Nishiyama, T. *et al.* Sororin mediates sister chromatid cohesion by antagonizing Wapl. *Cell* **143**,
814 737–749 (2010).

815 41. Yamada, T., Tahara, E., Kanke, M., Kuwata, K. & Nishiyama, T. Drosophila Dalmatian combines
816 sororin and shugoshin roles in establishment and protection of cohesion. *EMBO J.* **36**, 1513–

1527 (2017).

42. Rankin, S., Ayad, N. G. & Kirschner, M. W. Sororin, a substrate of the anaphase- promoting complex, is required for sister chromatid cohesion in vertebrates. *Mol. Cell* **18**, 185–200 (2005).

43. Schmitz, J., Watrin, E., Lénárt, P., Mechtler, K. & Peters, J. M. Sororin Is Required for Stable Binding of Cohesin to Chromatin and for Sister Chromatid Cohesion in Interphase. *Curr. Biol.* **17**, 630–636 (2007).

44. Ouyang, Z., Zheng, G., Tomchick, D. R., Luo, X. & Yu, H. Structural Basis and IP6 Requirement for Pds5-Dependent Cohesin Dynamics. *Mol. Cell* **62**, 248–259 (2016).

45. Ladurner, R. *et al.* Sororin actively maintains sister chromatid cohesion. *EMBO J.* **35**, 635–653 (2016).

46. Waizenegger, I. C., Hauf, S., Meinke, A. & Peters, J. M. Two distinct pathways remove mammalian cohesin from chromosome arms in prophase and from centromeres in anaphase. *Cell* **103**, 399–410 (2000).

47. Buheitel, J. & Stemmann, O. Prophase pathway-dependent removal of cohesin from human chromosomes requires opening of the Smc3-Scc1 gate. *EMBO Journal* vol. 32 666–676 (2013).

48. Gandhi, R., Gillespie, P. J. & Hirano, T. Human Wapl Is a Cohesin-Binding Protein that Promotes Sister-Chromatid Resolution in Mitotic Prophase. *Curr. Biol.* **16**, 2406–2417 (2006).

49. Zhang, N., Panigrahi, A. K., Mao, Q. & Pati, D. Interaction of sororin protein with polo-like kinase 1 mediates resolution of chromosomal arm cohesion. *J. Biol. Chem.* **286**, 41826–41837 (2011).

50. Dreier, M. R., Bekier, M. E. & Taylor, W. R. Regulation of sororin by cdk1-mediated phosphorylation. *J. Cell Sci.* **124**, 2976–2987 (2011).

51. Nishiyama, T., Sykora, M. M., Huis, P. J., Mechtler, K. & Peters, J. M. Aurora B and Cdk1 mediate Wapl activation and release of acetylated cohesin from chromosomes by phosphorylating Sororin. *Proc. Natl. Acad. Sci. U. S. A.* **110**, 13404–13409 (2013).

52. Liu, H., Rankin, S. & Yu, H. Phosphorylation-enabled binding of SGO1-PP2A to cohesin protects sororin and centromeric cohesion during mitosis. *Nat. Cell Biol.* **15**, 40–49 (2013).

53. Kitajima, T. S. *et al.* Shugoshin collaborates with protein phosphatase 2A to protect cohesin. *Nature* **441**, 46–52 (2006).

54. Hornig, N. C. D., Knowles, P. P., McDonald, N. Q. & Uhlmann, F. The dual mechanism of separase regulation by securin. *Curr. Biol.* **12**, 973–982 (2002).

55. Hagting, A. *et al.* Human securin proteolysis is controlled by the spindle checkpoint and reveals when the APC/C switches from activation by Cdc20 to Cdh1. *J. Cell Biol.* **157**, 1125–1137 (2002).

56. Wirth, K. G. *et al.* Separase: A universal trigger for sister chromatid disjunction but not chromosome cycle progression. *J. Cell Biol.* **172**, 847–860 (2006).

57. Sutani, T., Kawaguchi, T., Kanno, R., Itoh, T. & Shirahige, K. Budding Yeast Wpl1(Rad61)-Pds5 Complex Counteracts Sister Chromatid Cohesion-Establishing Reaction. *Curr. Biol.* **19**, 492–497 (2009).

58. Yang, C. *et al.* SWITCH 1/DYAD is a WINGS APART-LIKE antagonist that maintains sister chromatid cohesion in meiosis. *Nat. Commun.* **10**, (2019).

59. Zhang, N. & Pati, D. C-terminus of sororin interacts with sa2 and regulates sister chromatid cohesion. *Cell Cycle* **14**, 820–826 (2015).

60. Wu, F. M., Nguyen, J. V. & Rankin, S. A conserved motif at the C terminus of sororin is required for sister chromatid cohesion. *J. Biol. Chem.* **286**, 3579–3586 (2011).

61. McDowall, M. D. *et al.* PomBase 2015: Updates to the fission yeast database. *Nucleic Acids Res.*

43, D656–D661 (2015).

62. Feytout, A., Vaur, S., Genier, S., Vazquez, S. & Javerzat, J.-P. Psm3 Acetylation on Conserved Lysine Residues Is Dispensable for Viability in Fission Yeast but Contributes to Eso1-Mediated Sister Chromatid Cohesion by Antagonizing Wpl1. *Mol. Cell. Biol.* **31**, 1771–1786 (2011).

63. Furuya, K., Takahashi, K. & Yanagida, M. Faithful anaphase is ensured by Mis4, a sister chromatid cohesion molecule required in S phase and not destroyed in G1 phase. *Genes Dev.* **12**, 3408–3418 (1998).

64. Chen, Z., McCroskey, S., Guo, W., Li, H. & Gerton, J. L. A genetic screen to discover pathways affecting cohesin function in Schizosaccharomyces pombe identifies chromatin effectors. *G3 Genes, Genomes, Genet.* **2**, 1161–1168 (2012).

65. Matsuyama, A. *et al.* ORFeome cloning and global analysis of protein localization in the fission yeast Schizosaccharomyces pombe. *Nat. Biotechnol.* **24**, 841–847 (2006).

66. Yatskevich, S., Rhodes, J. & Nasmyth, K. Organization of Chromosomal DNA by SMC Complexes. *Annual Review of Genetics* vol. 53 445–482 (2019).

67. Mercier, R. *et al.* SWITCH1 (SWI1): A novel protein required for the establishment of sister chromatid cohesion and for bivalent formation at meiosis. *Genes Dev.* **15**, 1859–1871 (2001).

68. Alomer, R. M. *et al.* Esco1 and Esco2 regulate distinct cohesin functions during cell cycle progression. *Proc. Natl. Acad. Sci. U. S. A.* **114**, 9906–9911 (2017).

69. Zhou, L. *et al.* The N-Terminal Non-Kinase-Domain-Mediated Binding of Haspin to Pds5B Protects Centromeric Cohesion in Mitosis. *Curr. Biol.* **27**, 992–1004 (2017).

70. Liang, C. *et al.* A kinase-dependent role for Haspin in antagonizing Wapl and protecting mitotic centromere cohesion. *EMBO Rep.* **19**, 43–56 (2018).

71. Wutz, G. *et al.* ESCO1 and CTCF enable formation of long chromatin loops by protecting cohesinstag1 from WAPL. *Elife* **9**, (2020).

72. Li, Y. *et al.* The structural basis for cohesin–CTCF-anchored loops. *Nature* **578**, 472–476 (2020).

73. Haase, J., Bonner, M. K., Halas, H. & Kelly, A. E. Distinct Roles of the Chromosomal Passenger Complex in the Detection of and Response to Errors in Kinetochore-Microtubule Attachment. *Dev. Cell* **42**, 640-654.e5 (2017).

74. Dai, J., Sultan, S., Taylor, S. S. & Higgins, J. M. G. The kinase haspin is required for mitotic histone H3 Thr 3 phosphorylation and normal metaphase chromosome alignment. *Genes Dev.* **19**, 472–488 (2005).

75. Kurihara, D., Matsunaga, S., Omura, T., Higashiyama, T. & Fukui, K. Identification and characterization of plant Haspin kinase as a histone H3 threonine kinase. *BMC Plant Biol.* **11**, (2011).

76. Wang, F. *et al.* Histone H3 Thr-3 phosphorylation by haspin positions Aurora B at centromeres in mitosis. *Science (80-.).* **330**, 231–235 (2010).

77. Yamagishi, Y., Honda, T., Tanno, Y. & Watanabe, Y. Two histone marks establish the inner centromere and chromosome bi-orientation. *Science (80-.).* **330**, 239–243 (2010).

78. Goto, Y. *et al.* Pds5 Regulates Sister-Chromatid Cohesion and Chromosome Bi-orientation through a Conserved Protein Interaction Module. *Curr. Biol.* **27**, 1005–1012 (2017).

79. Eddy, S. R. Profile hidden Markov models. *Bioinformatics* vol. 14 755–763 (1998).

80. Altschul, S. F. *et al.* Gapped BLAST and PSI-BLAST: A new generation of protein database search programs. *Nucleic Acids Research* vol. 25 3389–3402 (1997).

81. Katoh, K. & Toh, H. Recent developments in the MAFFT multiple sequence alignment program.

Brief. Bioinform. **9**, 286–298 (2008).

82. Drozdetskiy, A., Cole, C., Procter, J. & Barton, G. J. JPred4: A protein secondary structure prediction server. *Nucleic Acids Res.* **43**, W389–W394 (2015).

83. Waterhouse, A. M., Procter, J. B., Martin, D. M. A., Clamp, M. & Barton, G. J. Jalview Version 2-A multiple sequence alignment editor and analysis workbench. *Bioinformatics* **25**, 1189–1191 (2009).

84. Cipak, L. *et al.* Generation of a set of conditional analog-sensitive alleles of essential protein kinases in the fission yeast Schizosaccharomyces pombe. *Cell Cycle* **10**, 3527–3532 (2011).

85. Dudas, A., Polakova, S. & Gregan, J. Chromosome segregation: Monopolin attracts condensin. *Current Biology* vol. 21 (2011).

86. Sabatinos, S. A. & Forsburg, S. L. Molecular genetics of schizosaccharomyces pombe. *Methods Enzymol.* **470**, 759–795 (2010).

87. Cipak, L. *et al.* An improved strategy for tandem affinity purification-tagging of *Schizosaccharomyces pombe* genes. *Proteomics* **9**, 4825–4828 (2009).

88. Kovacikova, I. *et al.* A knockout screen for protein kinases required for the proper meiotic segregation of chromosomes in the fission yeast Schizosaccharomyces pombe. *Cell Cycle* **12**, 618–624 (2013).

89. Polakova, S. *et al.* Dbl2 Regulates Rad51 and DNA Joint Molecule Metabolism to Ensure Proper Meiotic Chromosome Segregation. *PLoS Genet.* **12**, (2016).

90. Phadnis, N. *et al.* Casein Kinase 1 and Phosphorylation of Cohesin Subunit Rec11 (SA3) Promote Meiotic Recombination through Linear Element Formation. *PLoS Genet.* **11**, (2015).

91. Murashige, T. & Skoog, F. A Revised Medium for Rapid Growth and Bio Assays with Tobacco Tissue Cultures. *Physiol. Plant.* **15**, 473–497 (1962).

92. Clough, S. J. & Bent, A. F. Floral dip: A simplified method for Agrobacterium-mediated transformation of Arabidopsis thaliana. *Plant J.* **16**, 735–743 (1998).

93. Xiang, C., Han, P., Lutziger, I., Wang, K. & Oliver, D. J. A mini binary vector series for plant transformation. *Plant Mol. Biol.* **40**, 711–717 (1999).

94. Alexander, M. P. Differential staining of aborted and nonaborted pollen. *Biotech. Histochem.* **44**, 117–122 (1969).

95. Vignard, J. *et al.* The Interplay of RecA-related Proteins and the MND1–HOP2 Complex during Meiosis in Arabidopsis thaliana. *PLoS Genet.* **3**, e176 (2007).

96. Sims, J., Copenhaver, G. P. & Schlögelhofer, P. Meiotic DNA repair in the nucleolus employs a nonhomologous end-joining mechanism. *Plant Cell* **31**, 2259–2275 (2019).

97. Kurzbauer, M. T., Uanschou, C., Chen, D. & Schlögelhofer, P. The recombinases DMC1 and RAD51 are functionally and spatially separated during meiosis in Arabidopsis. *Plant Cell* **24**, 2058–2070 (2012).

98. Higgins, J. D., Sanchez-Moran, E., Armstrong, S. J., Jones, G. H. & Franklin, F. C. H. The Arabidopsis synaptonemal complex protein ZYP1 is required for chromosome synapsis and normal fidelity of crossing over. *Genes Dev.* **19**, 2488–2500 (2005).

99. Chelysheva, L. *et al.* AtREC8 and AtSCC3 are essential to the monopolar orientation of the kinetochores during meiosis. *J. Cell Sci.* **118**, 4621–4632 (2005).

100. Cromer, L. *et al.* Centromeric cohesion is protected twice at meiosis, by SHUGOSHINs at anaphase i and by PATRONUS at interkinesis. *Curr. Biol.* **23**, 2090–2099 (2013).

101. Ren, J. *et al.* DOG 1.0: Illustrator of protein domain structures. *Cell Research* vol. 19 271–273

(2009).

Competing Interest

The authors declare to have no competing interests.

Acknowledgements

J.G. was supported by the Austrian Science Fund (FWF) (grant P30516), the Slovak Grant Agency VEGA (1/0450/18 and 2/0026/18) and the Slovak Research and Development Agency (APVV-17-0130, APVV-18-0219, and APVV-16-0120). Research in the laboratory of P.S. was supported by the Austrian Science Fund (FWF) (I 1468-B16; Special Research Focus program "Chromosome Dynamics" F3408-B19; FWF Doctoral Program "Chromosome Dynamics" W1238-B20) and the Austria's Agency for Education and Internationalization (Ernst Mach Grant to TTN). Research in the laboratory of J.-M.P is supported by Boehringer Ingelheim, the Austrian Research Promotion Agency (Headquarter grant FFG-852936), the European Research Council under the European Union's Horizon 2020 Research and Innovation Programme (1020558), the Human Frontier Science Program (RGP0057/2018), and the Vienna Science and Technology Fund (LS19-029). J.- M.P. is also an adjunct professor at the Medical University of Vienna. We thank Vera Schoft and the Vienna Biocenter Core Facility (PlantS) for assistance in generating the *Atsororin* mutant line. We thank M. Yanagida, J.P. Javerzat and J. Gerton for sending yeast strains and B. Huraiova, L. Cipak and S. Polakova for help with yeast experiments.

Author Contributions

A.S. and J.-M.P. performed the bioinformatic analyses and identified putative *Sororin* homologs in eukaryotes. M.G., I.K., T.N. and J.G. conceived and performed the experiments with *S. pombe*. I.P.M. and P.S. conceived and performed the experiments with *A. thaliana*. T.T.N. generated the *A. thaliana sororin* mutant. I.P.M., J.G., J.-M.P. and P.S. analyzed the data and wrote the manuscript.

978 **Figure legends**

979 **Figure 1.** *S. pombe* Sor1 and *A. thaliana* AtSORORIN share sequence similarities with
980 metazoan Sororin proteins. **a** Domain architecture of Sororin and putative Sororin
981 orthologs. The Sororin domain is shown in blue, the cluster of positively charged
982 residues (lysine, arginine) in red, the KEN box in magenta and the FGF motif in yellow.
983 The domain graphs were created with the help of the domain illustrator (DOG 2.0 [101]). **b**
984 Alignment of the C-terminal Sororin domain. UniProt accessions are provided next to
985 the species names. Residues mutated in this study are indicated by asterisks. Secondary
986 structure prediction of *H. sapiens* and *S. pombe* are shown on the top and bottom,
987 respectively, where alpha helices are in red, and beta strands in green.

988 **Figure 2.** *S. pombe* Sor1 is involved in sister chromatid cohesion and its conserved
989 residues are important for Sor1 function and association with cohesin. **a** *sor1Δ* cells
990 show a weak cohesion defect which is partially suppressed by *wpl1Δ.* Wild type and
991 *sor1Δ* haploid cells expressing *cen2*-GFP were fixed and stained with antibodies against
992 tubulin and GFP and sister chromatid cohesion was analyzed in metaphase cells. Nuclei
993 were visualized by Hoechst staining. Means +/- standard deviations are shown.
994 Unpaired t-test was performed for statistical analysis (**p<0.01; ns – not significant). **b**
995 Negative synthetic growth interaction in *eso1ts sor1Δ* and *mis4ts sor1Δ* double mutants
996 are associated with chromosome segregation defects. Wild type, *sor1Δ*, *eso1-G799D*
997 *(eso1-ts)*, *eso1-G799D sor1Δ, mis4-242 (mis4-ts)* and *mis4-242 sor1Δ* haploid cells
998 expressing *cen2*-GFP were fixed and stained with antibodies against tubulin and GFP.
999 Nuclei were visualized by Hoechst staining. Samples were examined under the
1000 fluorescence microscope, and segregation of chromosome 2 marked by *cen2*-GFP was
1001 scored in late anaphase cells. Lagging chromosomes were identified as Hoechst-staining
1002 bodies between the poles of the spindle in late anaphase. Means +/- standard deviations
1003 are shown. Unpaired t-test was performed for statistical analysis (*p<0.05; **p<0.01). **c**
1004 Pds5-Myc co-immunoprecipitates with Sor1-Pk. Protein extracts were prepared from
1005 cycling wild type cells and cells expressing Sor1-Pk, Pds5-myc or both Sor1-Pk and
1006 Pds5-Myc, as indicated. Proteins bound to anti-V5 agarose beads, which bind the Pk tag
1007 on Sor1, were analyzed for Pds5-Myc by Western blotting using anti-Myc antibody. **d**
1008 Psm3-GFP co-immunoprecipitates with Sor1-Pk and this interaction is weakened by
1009 mutating conserved Sor1 residue D303. Protein extracts were prepared from cycling
1010 wild type cells and cells expressing Sor1-Pk, Psm3-GFP or both Sor1-Pk and Psm3-

GFP, as indicated. Proteins bound to anti-V5 agarose beads, which bind the Pk tag on Sor1, were analyzed for Psm3-GFP by Western blotting using anti-GFP antibody. Mutant protein Sor1-D303A-Pk co-immunoprecipitated with the Psm3-GFP protein less efficiently, as compared to wild type Sor1-Pk. **e** The four conserved residues in the Sororin domain are important for the Sor1 function. Strains with the indicated mutations were grown on YES medium for one day. Serial dilutions were spotted onto YES plates and incubated for 3 days at 25°C or 30°C. While expression of a wild type Sor1 rescued the growth defect of the *eso1-G799D sor1Δ* double mutant (*eso1-ts sor1-wt*), mutant Sor1 proteins carrying F299A, V302A, D303A or Y305A substitutions did not rescue the growth defect of *eso1-G799D sor1Δ* double mutants (*eso1-ts sor1-F299A, eso1-ts sor1-V302A, eso1-ts sor1-D303A, eso1-ts sor1-Y305A*).

Figure 3. Loss of WAPL rescues somatic defects of *Atsororin* mutants. **a** Schematic representation of *AtSORORIN* (AT3G56250) gene, with 5' and 3' UTRs (grey boxes), introns (black lines) and exons (black boxes), open reading frame (ATG/TAA, black), Cas9 target site (black triangle) and premature stop codon in mutants plans (TAA, red) indicated. **b** The severe growth restriction of homozygous *Atsororin* mutants plants (seedlings, scale bar = 5mm; mature plants, scale bar = 5 cm) is alleviated by loss of WAPL (*Atsororin wapl1-1 wapl2* triple mutants). Wild-type plants, *Atsororin*, *wapl1-1 wapl2* double mutants and *Atsororin wapl1-1 wapl2* triple mutants were grown side-by-side for comparison. **c** Images of root tips and entire seedlings (small pictures) of plants grown on media plates for two weeks. Root growth restriction (red bars) and loss of characteristic layering of the root meristem in *Atsororin* mutant plants are evident. These deficiencies are rescued by loss of WAPL (*wapl1-1 wapl2* double mutants). All plants were grown side-by-side for comparison. Scale bar = 1 mm. **d** Quantification of root growth of plants grown on media plates for two weeks. Unpaired Mann-Whitney test has been applied (*p<0.05; **p<0.01; ****p<0.0001; ns – difference not significant). **e** Loss of fertility in *Atsororin* mutant plants is only partially rescued by WAPL inactivation. All plants were grown side-by-side and genotypes are indicated. Images show representative, opened siliques and developing seeds. *Atsororin wapl1-1 wapl2* triple mutant plants have siliques with some seeds, which are mostly bigger than those formed in wild type-plants. Unpaired Mann-Whitney test has been applied (****p<0.0001). Scale bar = 1 mm. **f** Genotypes of offspring of self-pollinated *AtSORORIN* +/– plants. The homozygous *Atsororin* –/– genotype is strongly

underrepresented (chi-square analysis, p value indicated). **g** Genotyping the offspring of reciprocal crosses between *AtSORORIN* +/– and wild type plants indicates that only male, but not female, gametogenesis, is affected by the *Atsororin* mutation (Fisher's exact test, p values indicated). **h** Flower architecture is not affected by the lack of AtSORORIN whereas anther growth and pollen viability are severely disturbed. *Atsororin* single mutants and *Atsororin wapl1-1 wapl2* triple mutants develop smaller anthers with few viable pollen grains. All plants were grown side-by-side and genotypes are indicated. Scale bar flowers = 1 mm, scale bar anthers = 200 µm.

Figure 4. Somatic defects in *Atsororin* mutants are tissue-specific and WAPL-dependent. DNA was stained with DAPI (magenta) and fluorescence *in situ* hybridization (FISH) was performed to detect centromeric regions (green). **a** Spreads of root cell nuclei. Interphase, metaphase and anaphase stages were analyzed for wild-type plants and *Atsororin*, *wapl1-1 wapl2* and *Atsororin wapl1-1 wapl2* mutants. Scale bar = 10 µm. **b** Quantification of centromeric-FISH signals in interphase root nuclei. *Atsororin* mutants (n = 34) show a significantly higher number of signals than wild type (n = 93), *wapl1-1 wapl2* (n = 73) and *Atsororin wapl1-1 wapl2* (n = 59) (chi-square analysis; *p<0.05; **p<0.01; ****p<0.0001; ns – difference not significant). **c** Spreads of somatic cell nuclei from inflorescences. Interphase, prophase, prometaphase, metaphase and anaphase stages were analyzed for wild-type plants and *Atsororin*, *wapl1-1 wapl2* and *Atsororin wapl1-1 wapl2* mutants. Magnifications of signals at the sister centromeres are provided for prophase and prometaphase stages. Scale bar = 10 µm. **d** Quantification of centromeric-FISH signals observed in nuclei of cells from inflorescences at interphase. Quantification was performed on wild-type plants (n = 224) and *Atsororin* (n = 266), *wapl1-1 wapl2* (n = 238) and *Atsororin wapl1-1 wapl2* mutants (n = 236) (chi-square analysis; ****p<0.0001; ns – difference not significant). **e** Measurements of the physical distance between FISH signals of sister chromatid centromeres during prophase. *Atsororin* mutants (n = 39) show a significant increase in distance between sister centromeres when compared to wild type (n = 45), *wapl1-1 wapl2* (n = 37) and *Atsororin wapl1-1 wapl2* (n = 50). Unpaired t-test was performed (*p<0.05; ***p<0.001; ****p<0.0001). **f** Measurements of the physical distance between FISH signals at sister chromatid centromeres during prometaphase. *Atsororin* mutants (n = 55) show a significant increase in distance between sister centromeres when compared to wild type (n = 42), *wapl1-1 wapl2* (n = 46) and *Atsororin wapl1-1*

wapl2 (n = 49). Unpaired t-test was performed (****p<0.0001; ns – difference not significant).

Figure 5. Plants lacking AtSORORIN exhibit defects during male meiosis. Spreads of meiotic nuclei from wild-type plants and *Atsororin*, *wapl1-1 wapl2* and *Atsororin wapl1-1 wapl2* mutants. Meiotic progression until metaphase I, including homologous chromosome pairing and bivalent formation, appears normal in all genotypes. The number of DAPI-stained bodies is increased in mutants lacking AtSORORIN after metaphase I, yielding 10 chromatids in prophase II. Progression through meiosis II is therefore defective in *Atsororin* single mutants with the subsequent formation of unbalanced tetrads. Inactivation of WAPL does not rescue chromosome non-disjunction observed in anaphase II in the *Atsororin* single mutants. Scale bar = 10 µm.

Figure 6. Premature separation of centromeres during meiosis in *Atsororin* mutant plants. Fluorescence *in situ* hybridization experiment on male meiocytes with a probe directed against the centromeric regions (green) in wild-type plants and *Atsororin*, *wapl1-1 wapl2* and *Atsororin wapl1-1 wapl2* mutants. **a** Inactivation of *AtSORORIN* leads to premature loss of centromeric cohesion at the metaphase to anaphase transition during meiosis I. Inlays show magnifications of sister centromeric signals during metaphase I. Scale bar = 10 µm. **b** Magnifications of images depicting metaphase I stages for wild type plans, *Atsororin* single mutants and *Atsororin wapl1-1 wapl2* triple mutants. Premature splitting of centromeric signals is evident in the absence of AtSORORIN. Centromeres are stained in green and DNA is stained in magenta. Scale bar = 10µm. **c** Quantification of the number of centromeric signals from metaphase I to prophase II stages in wild type plants (n = 73) and *Atsororin* (n = 25), *wapl1-1 wapl2* (n = 22) and *Atsororin wapl1-1 wapl2* (n = 33) mutants. **d** Quantification of the number of centromeric signals at metaphase II in wild type plants (n = 13) and *Atsororin* (n = 12), *wapl1-1 wapl2* (n = 12) and *Atsororin wapl1-1 wapl2* (n = 15) mutants. **e** Quantification of the number of centromeric signals in tetrads (balanced: 4 nuclei with 5 centromere signals each) in wild type plants (n = 33) and *Atsororin* (n = 25), *wapl1-1 wapl2* (n = 28) and *Atsororin wapl1-1 wapl2* (n = 18) mutants.

Figure 7. Immunolocalization of the axis protein ASY1, the synaptonemal complex protein ZYP1 and the cohesin subunit SCC3 in male meiocytes during late zygotene in wild type plants and *Atsororin*, *wapl1-1 wapl2* and *Atsororin wapl1-1 wapl2* mutants.

1109 Absence of AtSORORIN does not influence their time of deposition or their relative
1110 localisation on meiotic chromosomes. Scale bar = 10 µm.

1111 **Table 1.** *S. pombe* strains and genotypes

Strain number	Genotype
MG1	*cen2(D107):kan-ura4+-lacO his7+::lacI-GFP*
MG2	*cen2(D107):kan-ura4+-lacO his7+::lacI-GFP sor1::kanMX*
MG3	*cen2(D107):kan-ura4+-lacO his7+::lacI-GFP wpl1::natMX*
MG4	*cen2(D107):kan-ura4+-lacO his7+::lacI-GFP sor1::kanMX wpl1::natMX*
MG5	*cen2(D107):kan-ura4+-lacO his7+::lacI-GFP eso1-G799D*
MG6	*cen2(D107):kan-ura4+-lacO his7+::lacI-GFP sor1::kanMX eso1-G799D*
MG7	*cen2(D107):kan-ura4+-lacO his7+::lacI-GFP mis4-242*
MG8	*cen2(D107):kan-ura4+-lacO his7+::lacI-GFP sor1::kanMX mis4-242*
MG9	*sor1-pk9::kanMX pds5-myc::kanMX*
MG10	*pds5-myc::kanMX*
MG11	*sor1-pk9::kanMX*
MG12	*sor1-pk9::kanMX psm3-GFP::natMX*
MG13	*sor1-D303A-pk9::kanMX psm3-GFP::natMX*
MG14	*sor1-GFP::kanMX*
MG15	*sor1-Flag::kanMX*
JG17331	*ade6-M216 lys1-37*
JG16900	*eso1-G799D*
JG16897	*sor1::kanMX eso1-G799D*
JG16904	*eso1-G799D sor1::sor1-wt::hphMX*
JG16879	*eso1-G799D sor1::sor1-F299A::hphMX*
JG16881	*eso1-G799D sor1::sor1-V302A::hphMX*
JG16883	*eso1-G799D sor1::sor1-D303A::hphMX*
JG16885	*eso1-G799D sor1::sor1-Y305A::hphMX*
MG13	*sor1::TAP::kanMX*
MG14	*sor1-F299A::TAP::kanMX*
MG15	*sor1-V302A::TAP::kanMX*
MG16	*sor1-D303A::TAP::kanMX*
MG17	*sor1-Y305A::TAP::kanMX*

1112 (other auxotrophic markers not scored)

1113 **Table 2.** Primers used in this study

Name	**Sequence (5' -> 3')**	**Utility**
35Sp_Fwd	CACTGACGTAAGGGATGACGCAC	PCR for genotyping BASTA gene
Basta_Rev	GAAGTCCAGCTGCCAGAAAC	
WAPL1.1LP	TCCAATTTAGTGAAACGTGGG	PCR for genotyping *WAPL1-1* T-DNA insertion line
WAPL1.1RP	ACACACTTGATTGAGAACCCG	
WAPL2LP	TCCAGCAAAACAGACAGGAAG	PCR for genotyping *WAPL2* T-DNA insertion line
WAPL2RP	CTCAAATCTGCGAACGAAGAG	
LBb1.3	ATTTTGCCGATTTCGGAAC	T-DNA border primer for T-DNA insertion lines genotyping
Sororin_geno_Fwd	ATTATCGTCTCAAGCTCTCTCG	PCR for amplifying *SORORIN* gene
Sororin_geno_Rev	GCAGACATACGGCGAGTTAC	
Sororin_sequencing	GCTCTCTCGAGCCTTCTTCA	Sanger sequencing of the PCR product of *SORORIN* gene
Sororin_compl_Fwd	TCGGTCCAAATATATCAACAGC	PCR for genomic AtSORORIN for complementation line
Sororin_compl_Rev	AAATCGCCACTTCTGTACGC	

1114

Figure 1

a

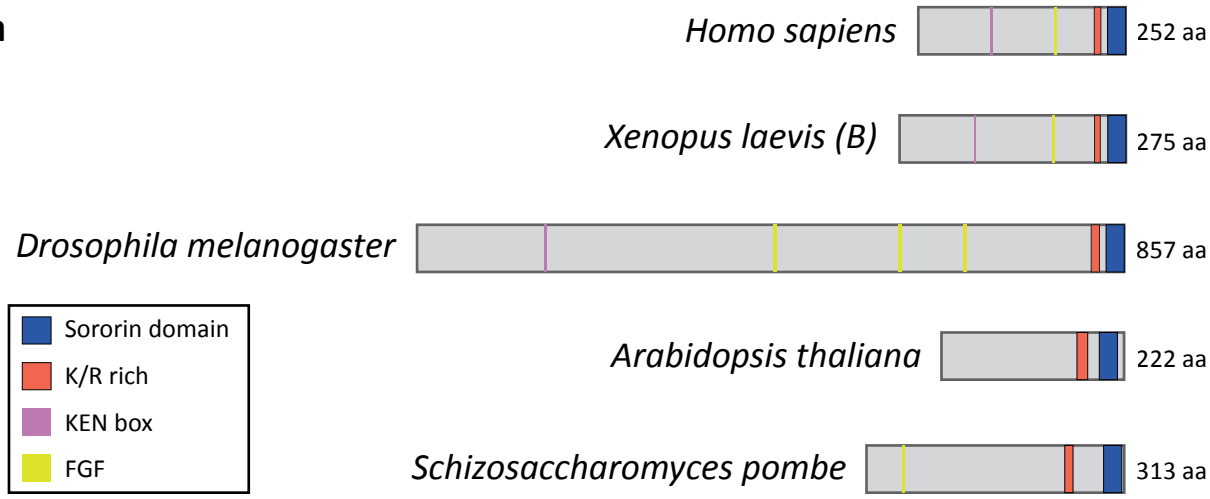

b

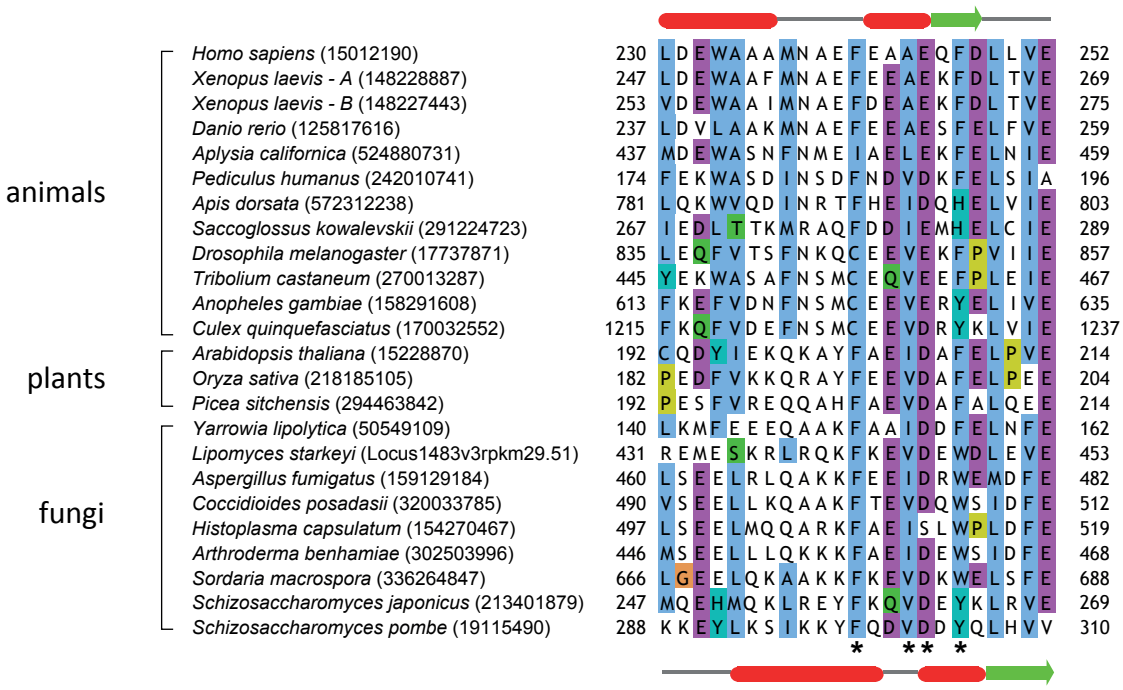

Figure 2

a

	cohesed sister centromeres	split sister centromeres	
wild type	59	41 (+/- 1,4)	**
sor1Δ	51	49 (+/- 3,5)	**
wpl1Δ	60	40 (+/- 1,7)	ns
wpl1Δ sor1Δ	58	42 (+/- 1,9)	ns

b

	normal segregation	missegregation	lagging chromosomes	
wild type	100	0	1 +/- 0,7	
sor1Δ	100	0	1 +/- 0,7	
eso1-ts	98	2 +/- 0,7	20 +/- 2,5	**
eso1-ts sor1Δ	94	6 +/- 1,4	33 +/- 4,4	**
mis4-ts	100	0	2 +/- 0,7	*
mis4-ts sor1Δ	98	2 +/- 0,7	4 +/- 1,0	*

c

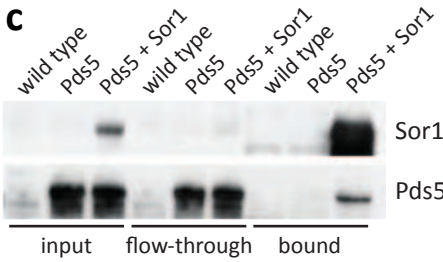

d

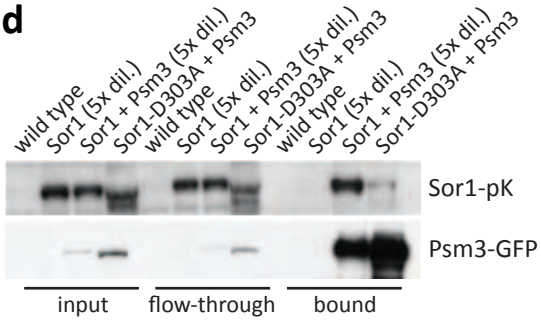

e

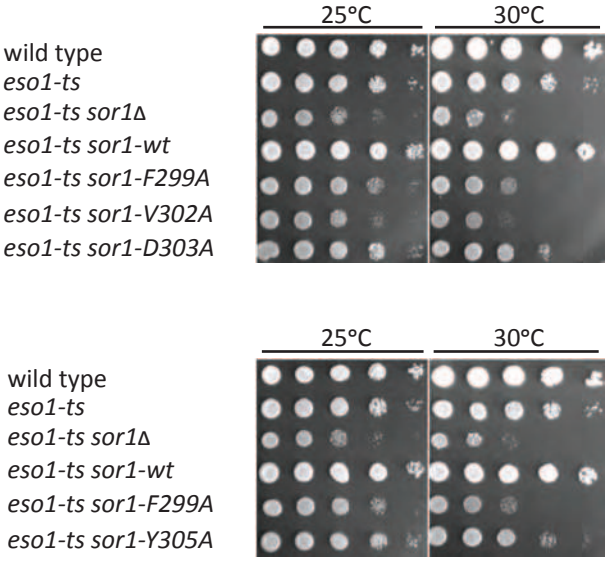

Figure 3

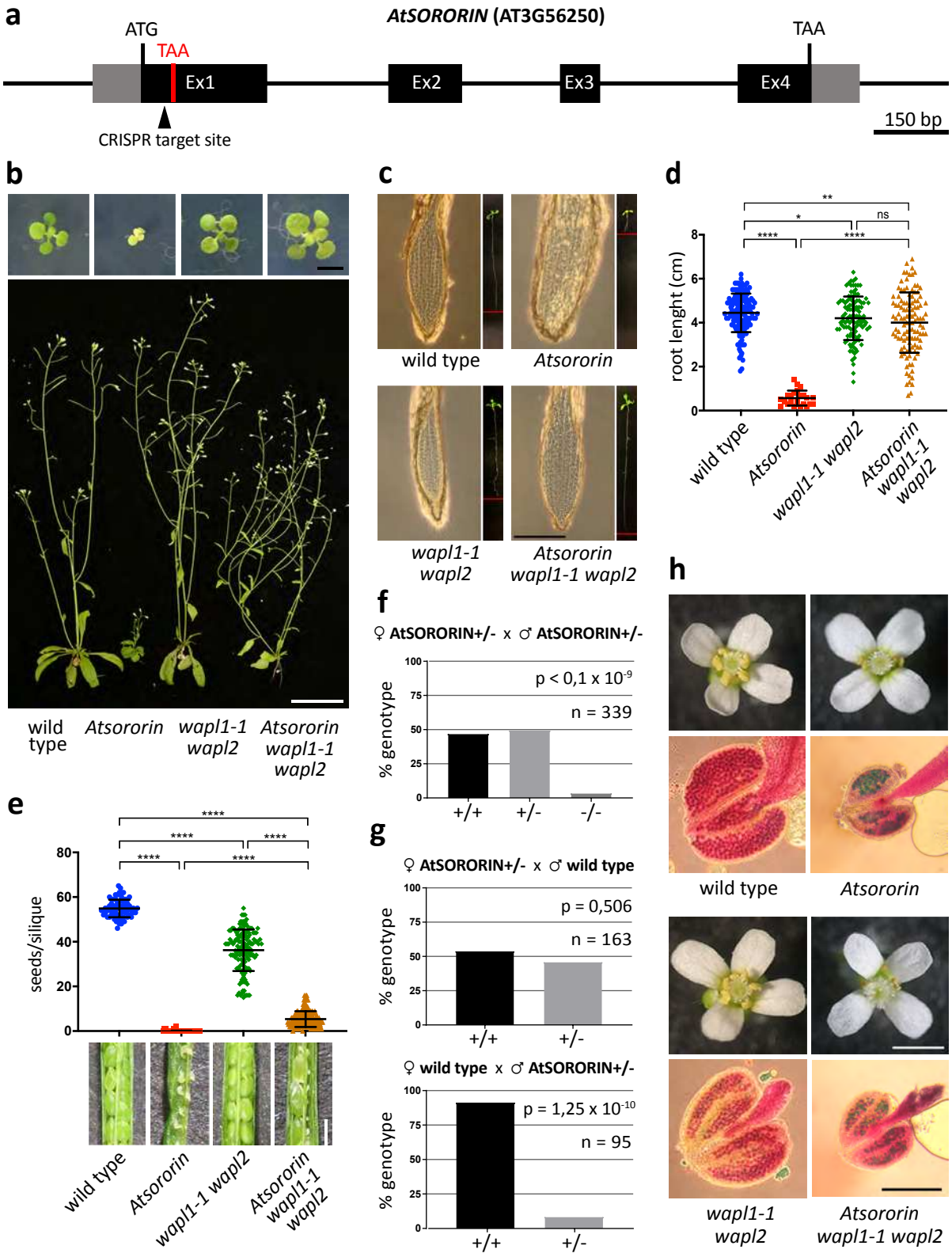

Figure 4

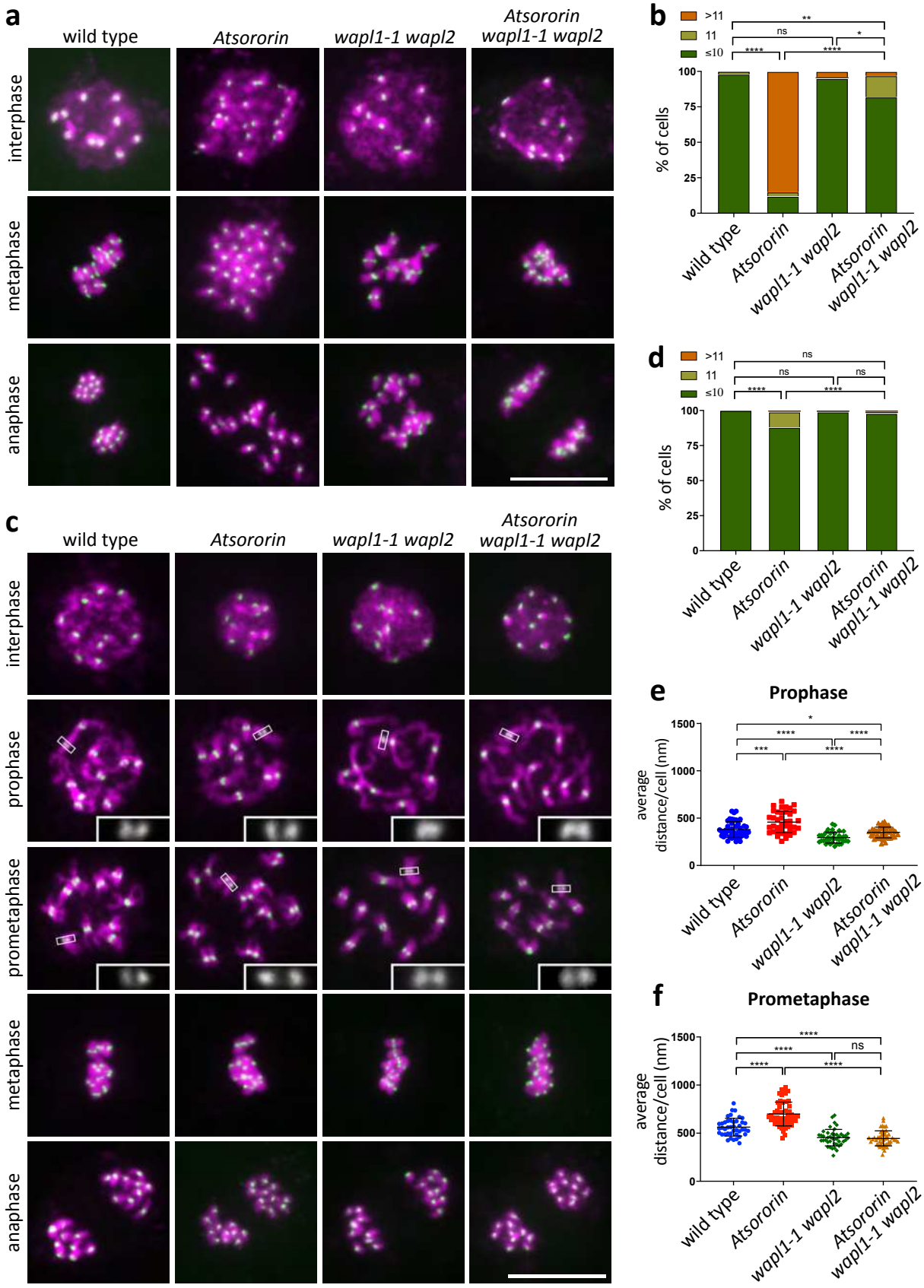

Figure 5

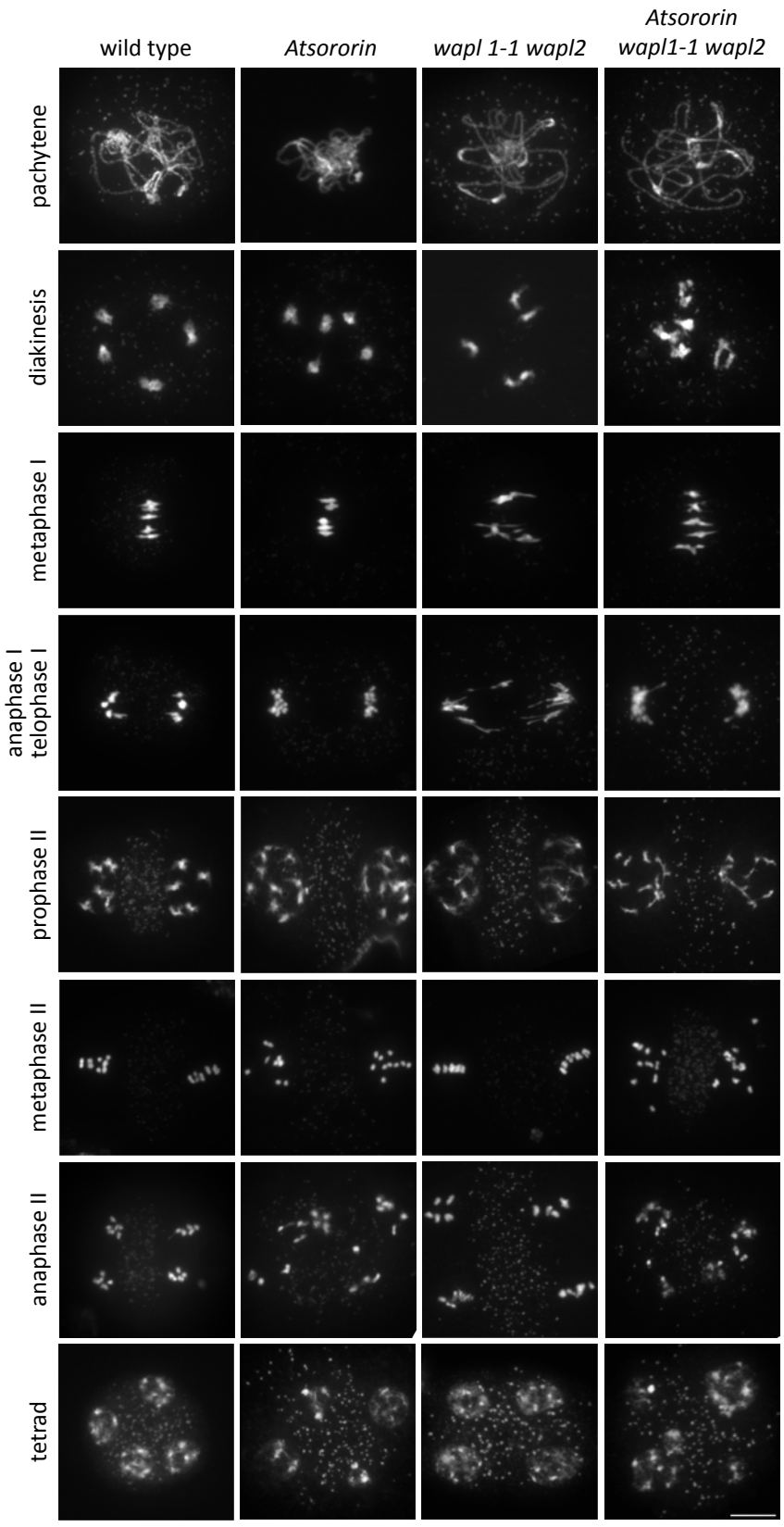

Figure 6

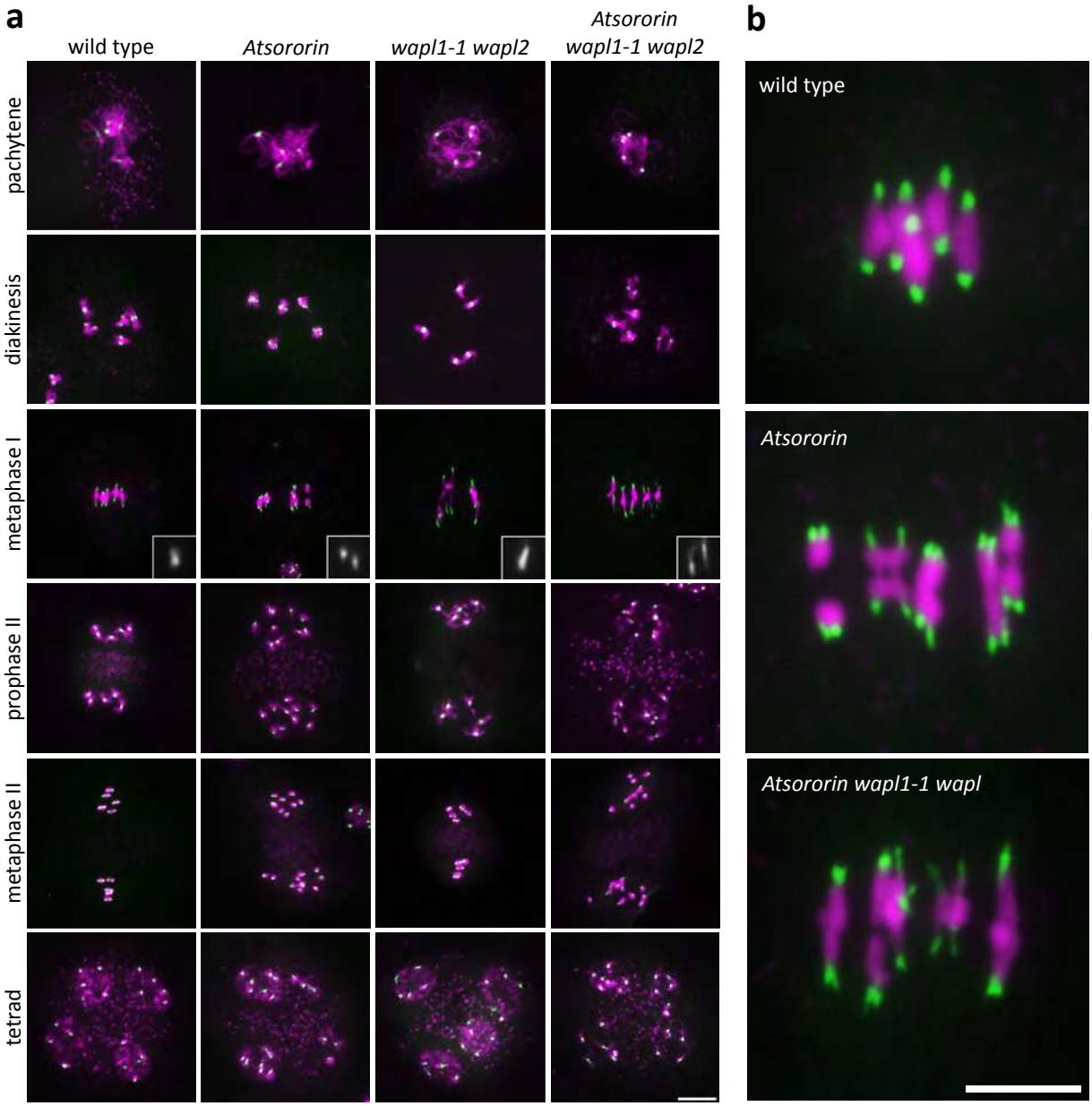

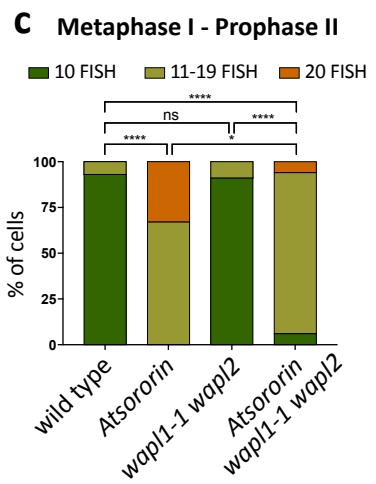

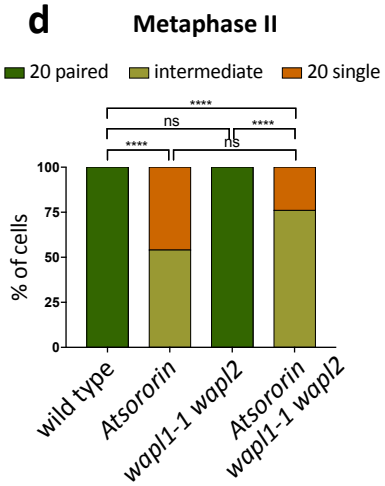

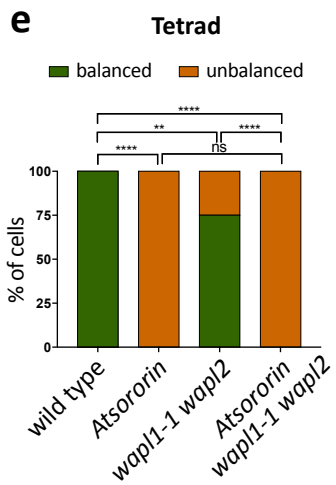

Figure 7

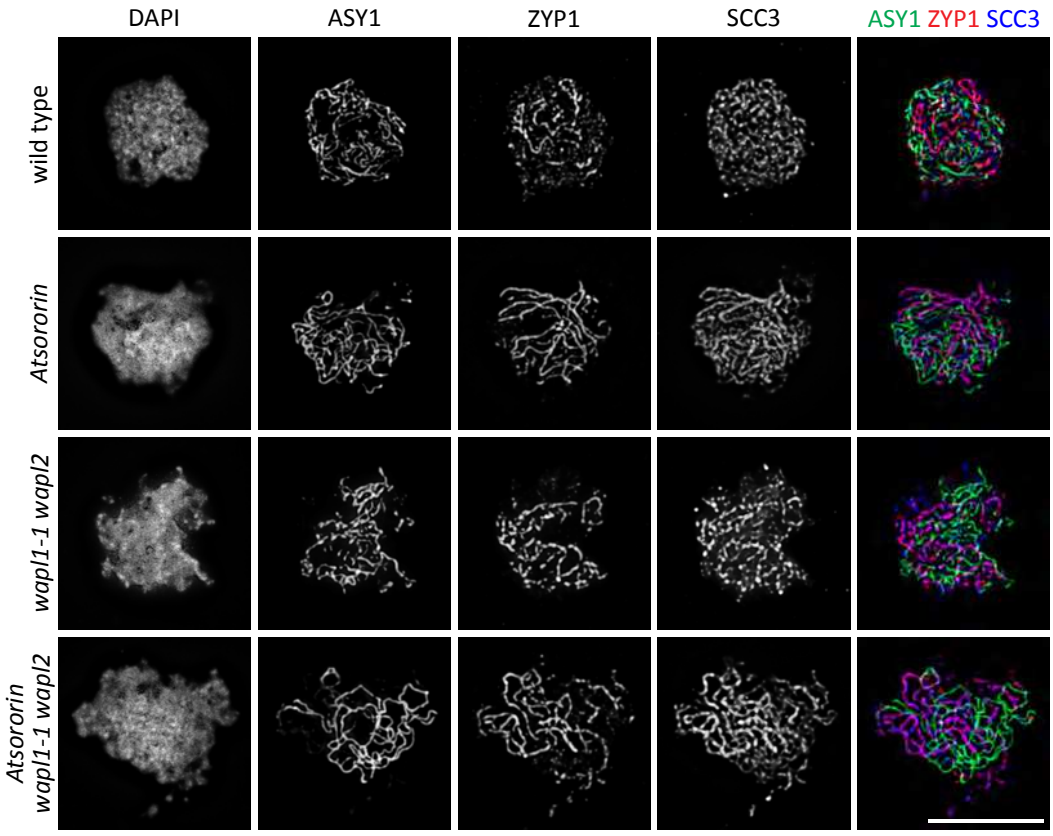

Supplementary information

Supplementary Figure 1 (supporting Figure 2)**.** Subcellular localization, APC/C degradation assay and expression analysis of *S. pombe* Sor1. **a, b** Sor1 localizes to nucleus throughout the cell cycle. Cycling *S. pombe* cells expressing Sor1-GFP were fixed, stained with DAPI, and analyzed by fluorescence microscopy (**a**). Cycling *S. pombe* cells expressing Sor1-Flag were fixed and stained with antibodies against Flag and tubulin. Nuclei were visualized by DAPI staining (**b**). **c** *in vitro* assay shows no evidence that Sor1 is an APC/C substrate. **d** Mutating conserved Sor1 residues only slightly reduces Sor1 protein levels. Proteins extracted from cycling cells were analyzed by gel electrophoresis and Western blotting using anti-tubulin antibodies. The TAP epitope was detected using PAP antibodies (rabbit antiperoxidase antibody linked to peroxidase).

Supplementary Figure 2 (supporting Figures 3 and 4)**.** Meiotic and somatic *Atsororin* mutant phenotypes can be complemented with the wild type *AtSORORIN* gene. **a** Overall plant architecture and fertility are wild type-like in the complemented transgenic plant line, but not in the *Atsororin* mutant. **b** Seed counts demonstrate nearly wild type-like fertility of the complemented transgenic plant line, but sterility in the *Atsororin* mutant. Unpaired Mann-Whitney test has been applied (****$p<0.0001$). Somatic defects in *Atsororin* mutants are tissue-specific and WAPL-dependent. DNA was stained with DAPI (magenta) and fluorescence *in situ* hybridization (FISH) was performed to detect centromeric regions (green). **c** Spreads of cell nuclei from rosette leaf cells. Interphase stages were analyzed for wild type plants and *Atsororin*, *wapl1-1 wapl2* and *Atsororin wapl1-1 wapl2* mutants. The number of centromeric signals is indicated in the top left corner. Scale bar = 10µm. **d** Quantification of centromeric-FISH signals in interphase leaf nuclei. *Atsororin* mutants (n = 52) have a significantly higher number of cells that have more than 10 signals, when compared to wild type (n = 84), *wapl1-1 wapl2* (n = 68) and *Atsororin wapl1-1 wapl2* (n = 82). Chi-square test was performed (****$p<0.0001$).

Supplementary Figure 3 (supporting Figure 7)**.** Immunolocalization of the axis protein ASY1 and the meiosis-specific cohesin subunit REC8 in male meiocytes during late zygotene in wild type plants and *Atsororin*, *wapl1-1 wapl2* and *Atsororin wapl1-1 wapl2* mutants. Absence of AtSORORIN does not influence their time of deposition or their relative localisation on meiotic chromosomes. Scale bar = 10 µm.

Supplementary Movie 1. Root tips from wild type plants display normal tissue organization and nucleus size.

Supplementary Movie 2. Root cellular organization and nucleus size are highly affected in *Atsororin* mutant plants.

Supplementary Movie 3. Plants with mutations in both genes encoding WAPL (*wapl1-1 wapl2*) develop normal roots compared to wild type plants.

Supplementary Movie 4. *Atsororin wapl1-1 wapl2 triple* mutant plants develop normal roots, indicating that the *wapl1-1 wapl2* mutations suppress the effect of the *Atsororin* mutation with respect to root development.

Supplementary Figure 1

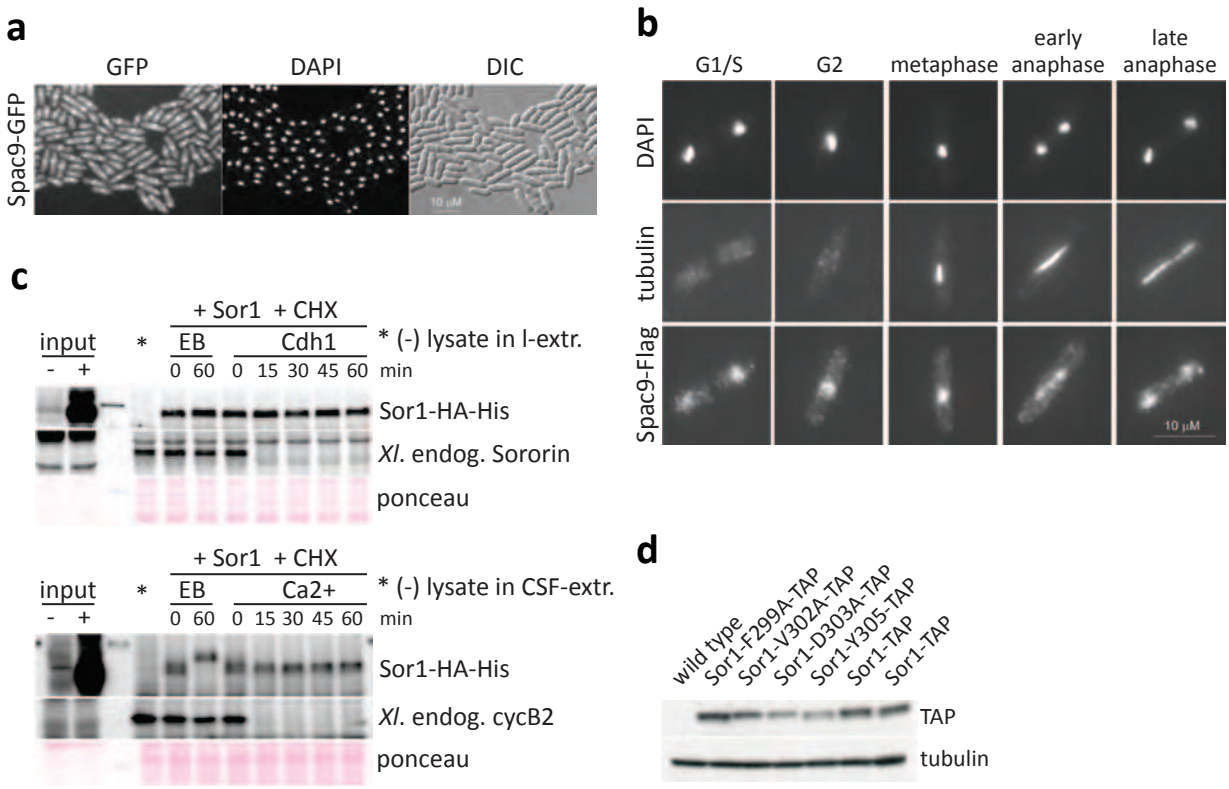

Supplementary Figure 2

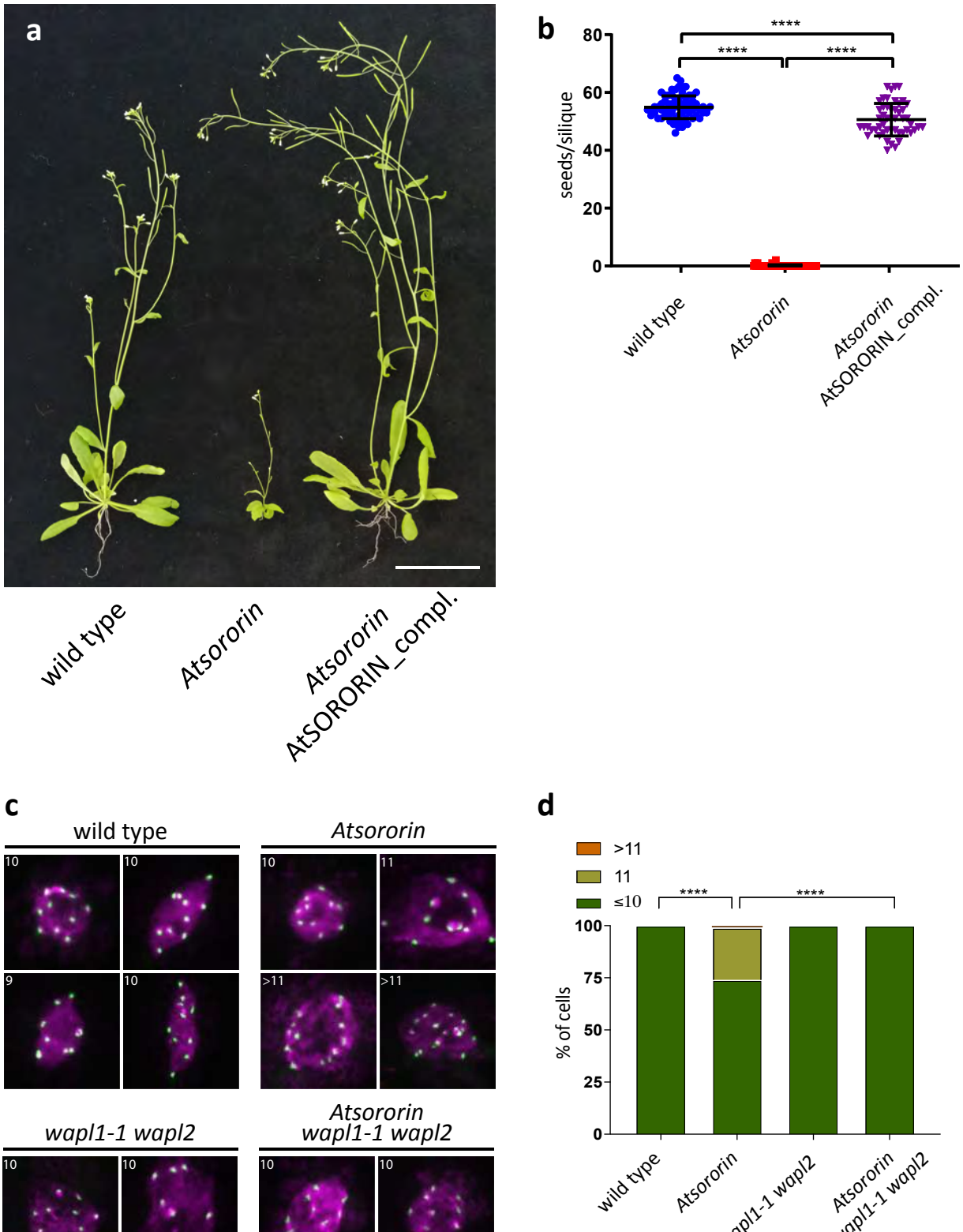

Supplementary Figure 3